Strategy of Regulating Electrolytes by Using Metal-organic Frame Work Channels for High-Energy-Density Li-ion Batteries

September 2020

CHANG ZHI

Strategy of Regulating Electrolytes by Using Metal-organic Frame Work Channels for High-Energy-Density Li-ion Batteries

Graduate School of Systems and Information Engineering
University of Tsukuba

September 2020

CHANG ZHI

ABSTRACT

The ever-increasing demand of electric portable devices and electric vehicles (EVs) calls for the development of high-efficient electrochemical energy conversion and storage devices that deliver higher energy-density puts. However, the dominantly graphite anode used commercialized lithium-ion batteries (LIBs) cannot satisfy current academic and industrial interest owing to their low energy density. Substituting the low theoretical specific capacity graphite anode in LIBs with lithium-metal which has high theoretical specific capacity and low electrochemical potential can effectively improve batteries' energy density. Pairing the lithium-metal with various high-voltage cathode materials is considered a promising strategy for the construction of high-energy-density lithium-metal batteries (LMBs). Yet, the development of next-generation high-energy-density LMBs was seriously limited by the disadvantages of currently existed electrolyte systems.

One of the most common inherent drawbacks of the existing electrolytes is the water molecules related issues, which we ascribe it as "external factor". Due to the existence of water molecules in LMB cell, HF would form during electrochemical cycling processes. The appearance of HF could accelerate transition metal dissolution TM (loss), electrolyte decomposition and lithium anodes degradation, thus was regarded as the culprit for capacity decay of LMBs/LIBs. More seriously, gaseous products produced within water contained electrolytes after electrochemical cycling would consequently result in increased internal pressure and severer electrolyte decomposition, and finally lead to possible safety hazards. Currently, as far as we know, there is no any effective and simple method to tackle with this annoying "external" problem. Herein, to solve this tricky issue, a CuBTC MOF based in-built

water scavenger within excellent water adsorb ability and strong chemical/physical stability was introduced into LMBs to scavenge water existed. Benefit from the use of MOF based water scavenger, we demonstrated significantly suppressed TM loss, electrolyte decomposition and Li anode degradation. Finally, after coupled MOF scavengers with various cathode materials, greatly improved electrochemical performances were obtained even under harsh condition of high water content electrolyte and evaluated temperature (500 ppm water, 55 ^{o}C). This is an important step to bring newly designed in-build MOF based in-built water scavenger from the laboratory to industrialization by reducing the manufacturing costs of lithium-ion batteries (LIBs) and improving their lifespan and safety simultaneously.

After the “external” factor had been successfully addressed, we begun to think further and looking forward to solve some “internal” factor (inherent defect) of electrolytes hat inhibit the application of high-energy-density LMBs. During the past few years, scientists mainly focus on using concentrated electrolytes to suppress the decomposition of electrolytes (mainly from solvents). Despite improved electrochemical performances were constantly reported, the fundamental electrolyte decomposition issues however, did not perfectly addressed. More importantly, those aforementioned electrolyte modification strategies usually involved in the extra dose usage of expensive solvents/additives, which means the cost for the fabrication of LMBs would largely increase. To further address the inherent electrolyte decomposition related problems existed in LMBs, much effective methods and strategies need to be carried out. Herein, confined inside metal-organic framework (MOF) channels, solvent-depleted carbonate electrolyte (Propylene Carbonate/LiTFSI (PC/LiTFSI) within MOF) which is compatible with both highly oxidative high-voltage cathodes and reductive Li-metal anodes was prepared. Different from conventional carbonate electrolytes, the obtained over-saturated carbonate electrolyte

possesses an over-saturated concentration. As a result, its reduction stability was inspiringly largely enhanced, thus rendering the obtained over-saturated carbonate electrolyte remarkably enhanced lithium compatibility (greatly improved Li//Cu symmetrical cell). Moreover, the oxidation stability was also improved (enlarged from original 4.5 volts to 5.4 volts). Coped with two high-voltage cathodes, ultra-stable high-energy-density lithium-metal batteries (NCM-811//Li; 5.0 V-class LCMO//Li) were finally achieved. More importantly, benefit from the unique electrolyte configuration, a cathode electrolyte interface (CEI) layer-free (CEI-free) cathode can be achieved, which is completely different from those using conventional carbonate electrolytes. The finding provides an enlightening insight to the development of lithium-friendly carbonate electrolyte and perfectly solving the long-lasting problem existed in high-energy-density LMBs.

Our findings emphasize the important role of MOFs in addressing some inherent drawbacks existed in LIBs/LMBs. We think that finding provides in this dissertation would provide an enlightening insight to the development of lithium-friendly carbonate electrolyte and perfectly solving the long-lasting problem existed in high-energy-density LMBs.

TABLE OF CONTENTS

LIST OF FIGURES

Chapter 1. General introduction

1.1 Increasing demands for energy storage technologies

Owing to the fast development of various industries, our society enjoyed great progress during the past decades. However, despite the big positive changes in our daily lives, there are also tremendous issues and challenges like the fossil energy crisis in recent years and the deteriorating global environmental problems.[1, 2] This urgent situation enables countries all over the world call for environmental friendly green energy on the agenda as shown in **Figure 1.1**.

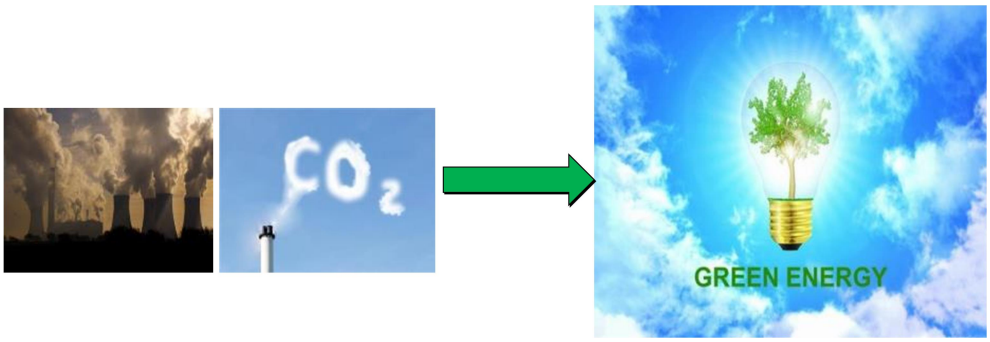

Figure 1. 1 Increasing deteriorate environment issues call for green energy. Pictures are from www.google.com/imghp?hl=zh-cn.

Technologies like wind turbine and solar energy are expected to alleviate those urgent crisis and detrimental environmental problems. Although the renewable clean energy can be collected, the collection of the clean energy is of great significance in order to fully use these forms of energy.[3] As shown in **Figure 1.2**, battery energy storage can help deal with the intermittent nature of renewables such as solar and wind energy. As an energy storage and conversion device for various new energy vehicles and electronic equipment, batteries have a top priority and affect the future of new energy vehicles and even the entire human society.[4] In the global situation of continuous energy shortage and increasing environmental pollution, how to efficiently

use existing resources, as well as electrochemical equipment for energy storage and conversion, improve the range of new energy electric steam.[5]

Figure 1. 2 Battery energy storage can help deal with the intermittent nature of renewables such as solar and wind energy. Picture is from www.google.com/imghp?hl=zh-cn.

Batteries, especially the Li-ion batteries (LIBs) are widely used in modern society in fields like tremendous electronic applications and even various electrical vehicles and railway systems as shown in **Figure 1.3**.[6-9] Since its commercialization, LIBs have had a huge impact on the world economy and people's lifestyles. Due to their relatively high energy density, lithium-ion secondary batteries are often used in various electronic products and defense equipment.[7, 10-12] However, the increasing rise and development of various types of electronic equipment have placed higher demands on the service life and energy density of various energy storage devices.[13-15] Therefore, the problems of the low specific capacity and short cycle life of various existing LIBs need to be solved urgently.

Figure 1. 3 The applications of Li-ion batteries in our daily life.[16]

1.2 Lithium-ion batteries (LIBs)

As can be found in **Figure 1.4**, for a conventional Li-ion battery (LIB), it composed of four different parts: anode, cathode, separator and electrolyte. Typically, cathode materials are commercialized LiM_xO_y (e.g. $LiNi_{0.5}Mn_{1.5}O_2$, $LiNi_xCo_yMn_zO_2$ (NCM, 811, 622, 333), $LiNi_xCo_yAl_zO_2$ (NCA), $LiMn_2O_4$, $LiFePO_4$).[10, 11, 17, 18] All of them can afford lithium interaction/extraction during discharge/charge processes. Anode material is dominated graphite, which is also based on lithium intercalation/extraction mechanism during discharge/charge processes. Sandwiched between cathode and anode, separator is typically porous materials like Celgard, PP, PE and even glass fiber. Inserted inside the gap between cathode and anode, separator is used to isolate the cathode and anode and prevent shortcut of cells while at the same time it allows lithium-ions to transfer normally from one side to another side.[9, 19] Electrolyte used in LIBs is generally carbonate-based electrolyte, which facilitates lithium ions to transport in it from one electrode to another one.[20, 21] The working

mechanism of LIB was explained in detail as shown below:

(1) For charging process, lithium ions are extracted from cathode material and then insert into graphite anode while at the same time electrons pass through external circuit, with the equations:

(2) For discharging process, lithium ions are extracted from graphite anode and then insert into cathode material.

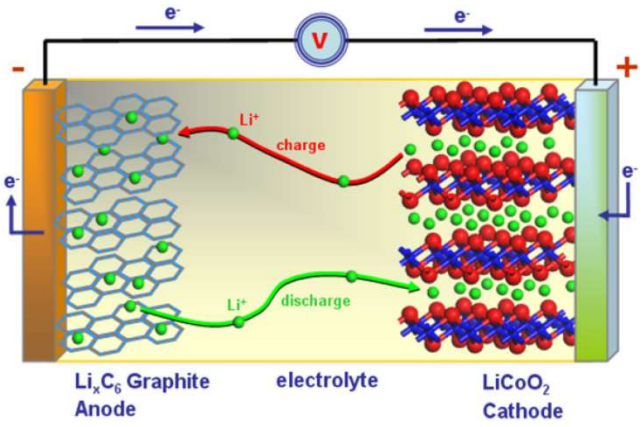

Figure 1. 4 Schematic illustration of a Lithium-ion battery (LIB).[7] Reproduced with permission from ref. 7. Copyright 2012, Elsevier Inc.

This process is reversible with lithium ions transported between cathode and anode like a rocking chair, this is the reason it was named as rocking chair batteries. Owing to the highly reversibility of the lithium intercalated/extracted from electrodes during discharge/charge processes, LIBs have enjoyed great commercial successes in the modern society. However, due to the limited specific capacity of the graphite anode (372 mAh/g), the energy-density of commercial LIBs was largely restrained, which hindered their practical applications in fields that required higher power-density.[22, 23] Generally, the output energy density of the LIB-full cell was calculated based on the formula shown below:

Output Energy (Wh/kg) = Cell voltage (V) * Capacity (mAh/g)

For example, when graphite anodes were used, a low energy-density below 250 Wh/kg was finally obtained restricted by the low capacity of graphite. Therefore, in

order to increase the output energy of the LIBs, we can replace the electrode materials with higher voltage platform or substitute the electrode materials with higher specific capacity.

1.3 Lithium-metal batteries (LMBs)

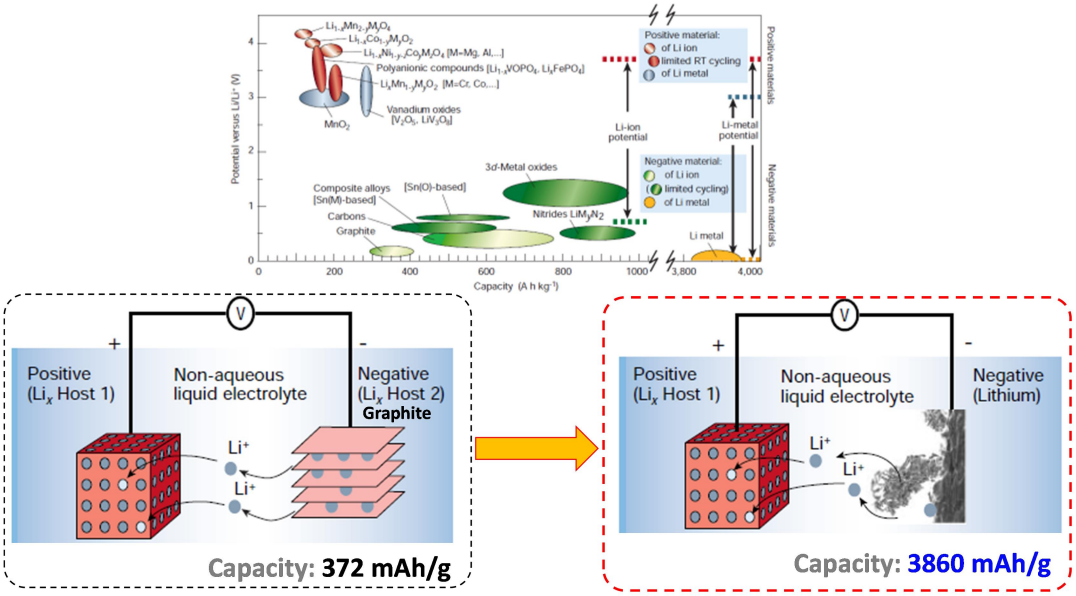

Figure 1. 5 The output voltage values for Li-ion cells or Li-metal cells. Schematic illustration of rechargeable Li-ion battery and rechargeable Li-metal battery (the picture of the dendrite growth at the Li surface was obtained directly from in situ scanning electron microscopy measurements).[9] Reproduced with permission from ref. 9. Copyright 2001, Springer Nature.

Replacing the low capacity graphite anode with high specific capacity lithium-metal (3860 mAh/g) can largely improve the output energy density of cells as shown in **Figure 1.5**.[15, 24-26] Coupling various high-voltage cathode materials with metallic lithium can effectively enhance the energy-density of lithium-metal batteries (LMBs).[27-29] For example, recently, tremendous scientific researchers have reported the constructing of high-energy-density LMBs after replacing graphite anode with lithium-metal anode. Owing to the high specific capacity and low potential of the

metallic lithium, LMBs with high output energy above 500 Wh/kg were achieved.[30]

1.4 Problems and challenges in high-energy-density LMBs

However, the lithium metal anode is a double-edged sword, since possesses extremely high capacity which is the most important fact that improve the energy-density, the limited life span, and low coulombic efficiencies (CEs), however, significantly backlash its most sparking characteristics. As shown in **Figure 1.6**, when used as anode in LMBs, lithium metal is vulnerable and tends to experience serious reregulated growth of dendritic lithium, which would constantly consume electrolytes and covered by uneven solid electrolyte interphases (SEI) and resulted in low coulombic efficiency (CE).[14, 27, 28, 31] Low CE of lithium anode would consequently largely deteriorate both the energy-density and cell cycling lifespan of LMBs. More seriously, the uncontrollable growth lithium dendrite can penetrate the separator which could even lead to potential safety hazards.[32-34]

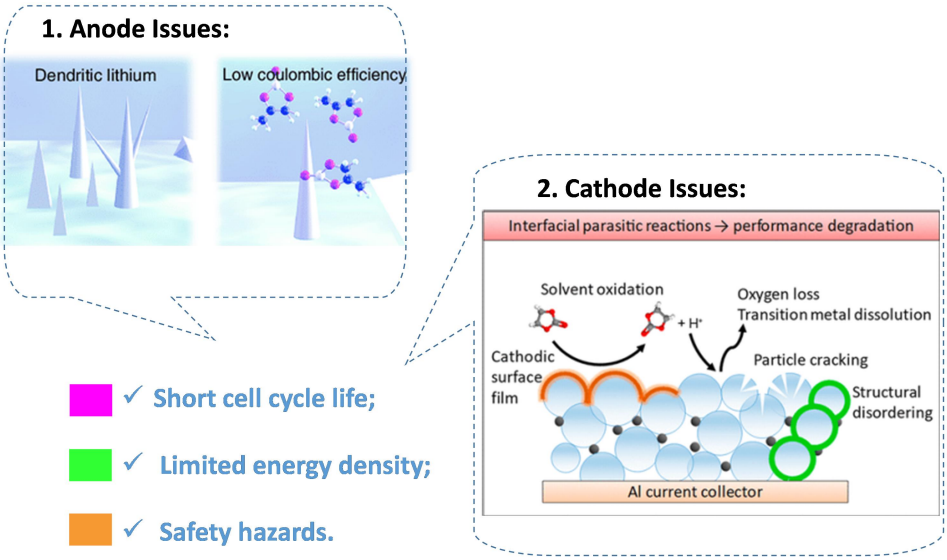

Figure 1. 6 Problems and challenges in high-energy-density lithium-metal batteries (LMBs).[35, 36] Reproduced with permission from ref. 35. Copyright 2019, Wiley-VCH. Reproduced with permission from ref. 36. Copyright 2019, American Chemical Society.

Moreover, since various high-voltage cathodes were employed to construct the high-energy-density LMBs, detrimental issues and challenges occurred on the cathodes can also largely influence the performances of the full cell which also deserve out attentions.[37-39] To be more specific, transition metal dissolution (TM loss), particle carking, structure disordering of cathode materials can all deteriorate the cathode stability and damage the performance of LMBs finally. Actually, those cathode side problems can be ascribed to the electrolyte-related parasitic reactions, which induced by electrolyte decompositions.[40, 41] Electrolyte oxidative products like HF/H^+ was reported can etching the cathode surface, which then lead to serious TM loss. The dissolved transition metal ions, then crossover to the anode and passive the lithium surface as shown in **Figure 1.6**.[42, 43]

In summary, both the cathode side issues and anode side problems can lead to the final limited energy-density and cell life. To effectively address these long-lasting and annoying obstacles, researchers from all over the world have reported various methods for high-energy-density LMBs. Among those methods and strategies, modifying electrolytes was regarded as an effective way to solve the detrimental problems existed in LMBs. For example, Yamada group[23, 44] and Zhang group[41-43, 45] have reported using highly-concentrated electrolyte in LMBs to suppress the electrolyte decomposition related side-reactions and obtained highly improved electrolyte performances in terms of capacities and cycling spans. Multiple electrolyte additives were also employed to stabilize the electrode/electrolyte interphases in LMBs.[45] F-doped/P-doped additives were designed to forming stable interfaces aiming to prolong the cycling life and safety of high-voltage LMBs.

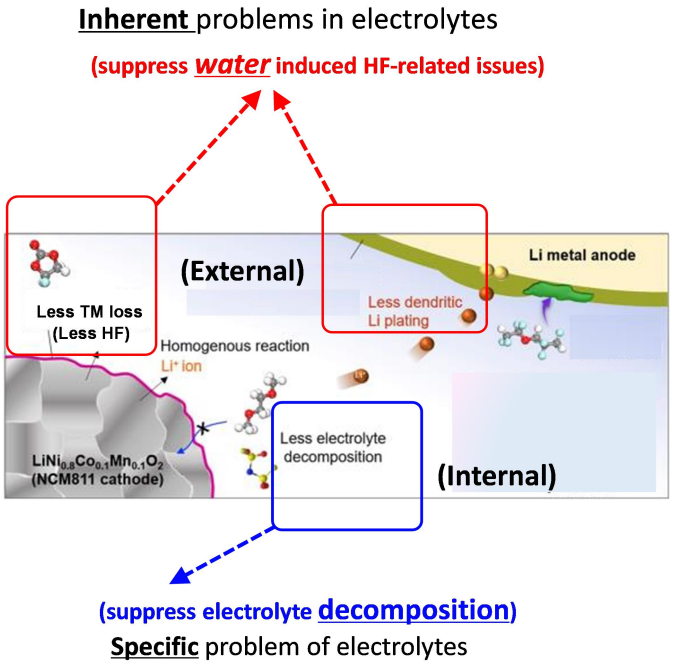

Figure 1. 7 Addressing electrolyte-related issues in high-voltage LMBs.[46] Reproduced with permission from ref. 46. Copyright 2020, Elsevier Inc.

Despite improved electrochemical performances were constantly reported, the fundamental electrolyte decomposition issues however, did not perfectly addressed. More importantly, those aforementioned electrolyte modification strategies usually involved in the extra dose usage of expensive solvents/additives, which means the cost for the fabrication of LMBs would largely increase.[21, 23] To further address the inherent electrolyte decomposition related problems existed in LMBs, much effective methods and strategies need to be carried out.[38, 47, 48]

As demonstrated in **Figure 1.7**, the electrolyte decomposition related issues can be generally divided into two different parts: (1) electrolyte residuals induced decompositions (noted as external one) and (2) electrolyte solvent deduced decompositions (defined as internal one). For example, a common phenomenon: the HF attack related issues, which can cause serious transition metal dissolutions, electrolyte solvents parasitic reactions and cathodes/anodes degradations, were actually induced by water residuals existed in LMBs.[37, 38] This problem is the primary

obstacle for the achieving of long cycle life high-energy-density LMBs.[32, 49, 50] If this fundamental issue can be perfectly addressed, then we can fully focus our attention in solving the specific decomposition of electrolyte solvents themselves in LMBs as shown in **Figure 1.7** (blue highlighted). Therefore, this dissertation is focus on solving both the inherent external drawbacks and specific electrolyte solvents decompositions in high-energy-density LMBs.[51-53] We would like to address the common existed water-related external issues firstly before the specific electrolyte solvent decomposition is solved.

1.5 Motivation and targets of this dissertation

1.5.1 Motivation of this dissertation

The growing demand for electric portable devices and electric vehicles requires the development of efficient electrochemical energy conversion and storage devices that can provide higher energy density. However, graphite anodes, which are mainly used in commercial lithium-ion batteries, cannot meet current academic and industrial interests due to their low energy density. Replacement of low theoretical specific capacity graphite anodes with lithium metals can effectively improve the energy density of batteries. Coupling lithium metal anodes with multiple high-voltage cathode materials is regarded as a bright method to build high-energy-density lithium metal batteries (LMB). However, the development of the high-energy-density LMBs is severely limited by the shortcomings of the electrolytes used in LMBs. Therefore, to improve both the energy density and lifespan of LMBs, strategies should be implemented to solve those detrimental issues.

However, the electrochemical performance of LMBs is mainly limited by the constant dissolution of harmful transition metals (TM loss) in high-voltage cathodes during electrochemical cycling. The detrimental TM loss found in LMBs can be attributed to the electrodes corrosion caused by HF, which is worsened especially when cycling under high voltage platform and high temperatures. The formation of HF was mainly induced by the hydrolysis of electrolytes due to the existed irremovable water traces in electrolytes. More seriously, the formation of various gaseous products caused by cathodic hydrogen evolution reaction (HER) and anodic oxygen evolution reaction (OER), which can also be ascribed to the existence of water in electrolyte, and lead to increased internal pressure and intensified electrolyte decomposition, eventually resulting in poor electrochemical performance and

potential safety hazards. Therefore, in order to extend the life and improve the safety of the LMBs, it is hence of great significance to reduce the water contained in electrolytes. However, conventional water removal processes are rigid one-time pre-treatments in drying electrolytes, thus only water already existed in electrolytes are expected to be removed while the subsequent continuously accumulated water upon cell fabrication and electrochemical cycling cannot be extruded. Hence, strategies which are simple, cheap while enable remarkable and continuous in-built water removal effects during battery cycling are anxiously desired for LIBs.

On the other hand, even the water-related serious problems existed in high-energy-density LMBs were effectively addressed by using MOF based in-built water scavengers, some inherent drawbacks of existing electrolytes, however, are still existed and damage the performance of LMBs. For example, ether-based electrolyte, although are highly compatible with metal Li, yet cannot be used as a working electrolyte for high-voltage LMB due to its poor oxidative stability (typically below 4.0 volts). In contrast, although carbonate-based electrolytes can be coupled with high-voltage cathode materials (greater than 4.0 V), unfortunately, they are not compatible with Li anodes, which will lead to severe growth of dendritic Li and thus pose a safety hazard. Therefore, this problem overshadows the development of long-life high energy density LMBs. Addressing the shortcomings of conventional electrolytes can fulfill the final goal of improving the energy-density of LMBs.

1.5.2 Target of this dissertation

The targets of this dissertation on using metal-organic frameworks (MOFs) to suppress electrolyte decomposition issues in high-energy-density lithium-metal batteries (LMBs) are as follows:

The first target is to address the fundamental external water induced HF/H^+

related electrolyte decompositions and the corresponding parasitic reactions in high-voltage LMBs. Generally, there are several different methods and procedures in factory scale to extrude water/moisture existed in commercial liquid electrolytes and water molecules adsorbed during cell fabrication processes. Unfortunately, owing to traditional water removal methods are often rigid one time treatments towards electrolytes, the unsustainable water removal effects and the insufficient water removal effectiveness however, make them unable to fully extrude water and accumulated constantly during electrochemical cycling processes. Hence, we focus on the representative MOF ($Cu_3(BTC)_2$) with excellent water adsorbing ability and investigate its water scavenging ability and the corresponding influences towards high-voltage LMBs.

After the first target is achieved, we start to think further and looking forward to solve some specific problems which closely related to the decomposition of electrolyte solvents themselves in high-voltage LMBs. So the second target is to suppress the electrolyte decomposition on both cathode and anode materials of LMBs and consequently improve the reversibility of lithium-metal anodes, and promote the realizing of cathode CEI-free high-energy-density LMBs. As discussed before, electrochemical stability of electrolytes is the one of the most important factor to maintain electrodes stability of high-energy-density LMBs. This guides us the direction and gives us inspiration. Therefore, it is of great significance to design electrolyte with much stable electrochemical stability aiming to achieve stable high-energy-density LMBs. Possessing various sub-nano channels, we hope MOF can fulfill this goal and regulated the configuration of electrolytes which confined inside its channels.

1.5.3 Outline of this dissertation

This dissertation contains five chapters illustrated as following:

Chapter 1 is a general instruction for the whole dissertation. In this chapter, the background of the increasing demands for energy storage technologies is discussed. Some battery technologies are compared, suggesting that Li-ion batteries (LIBs) are the most successful choice. Then, the disadvantages of the conventional LIB are further introduced compared with Lithium-metal batteries (LMBs), which present much higher specific capacity. Moreover, the challenges and problems of high-energy-density LMBs we also discussed. Finally, we present our motivation and provide our method of how to deal with the problems in high-energy-density LMBs.

Chapter 2 is the experimental section of Chapter 3 and Chapter 4. In this chapter, the synthesized method, testing condition, main operation steps and highlights of this dissertation are all introduced in detail.

Chapter 3 is the work about the addresses detrimental issues induced by water existed in carbonate electrolyte for high-voltage lithium-metal battery using metal-organic framework (MOF) based in-built water scavengers. In this chapter, various physical characterization technologies such as ICP, NMR and XPS are employed for a high-voltage LMBs to investigate the largely suppressed water-induced HF-related side-reactions. By using the prepared MOF based in-built water scavengers, water-induced HF-related side-reactions including transition metal dissolution, electrolyte decomposition and lithium-metal degradation were greatly inhibited. Electrochemical results are consistent well with our experimental observation.

Chapter 4 is the work about achieving a new over-saturated carbonate electrolyte inside MOF channels and the corresponding improved the capacity stability of high-energy-density LMBs and CEI-free cathode surface. In this chapter, a new

carbonate electrolyte with unique over-saturated electrolyte configuration is reported. The rational designed over-saturated electrolyte has advantages of enhanced both cathodic and anodic stability. Benefit from this unique configuration of the prepared over-saturated electrolyte, excellent Li reversibility is achieved. As a result, enhanced electrochemical performances of high-energy-density LMBs are obtained by coupling it with high-voltage cathode and lithium anode.

Chapter 5 is the general conclusions and perspective for future research in this field.

Chapter 2. Experimental section

2.1 Experimental section of Chapter 3

2.1.1 Preparation of $LiNi_{0.5}Mn_{1.5}O_4$ (LNMO) spinel cathode

(1) Preparation of $MnCO_3$ microspheres

Firstly, we thoroughly mixed 1.014 g manganese sulphate ($MnSO_4 \cdot H_2O$, Wako Pure Chemical Industries Ltd.) and sodium bicarbonate ($NaHCO_3$, 4.64 g, Wako Pure Chemical Industries Ltd.) in 2400 mL water, respectively. Then, 40 mL ethanol was added to the $MnSO_4$ solution under vigorous magnetic stirring, followed by the adding of the $NaHCO_3$ solution. The mixed solution was then aged for about 3 hours at room temperature (25 °C). The obtained $MnCO_3$ was then further centrifuged and washed for 3 times using water and alcohol solution, respectively, and then vacuum dried at 80 °C for 2 hours.

(2) Synthesis of yolk-structured MnO_2 microspheres

0.4 g the above obtained $MnCO_3$ microsphere was then dispersed into 80 mL water uniformly followed by stirred for 1 hour. Then 40 mL $KMnO_4$ solution (0.032 mol/L) was carefully added and vigorously stirred for 1 hour. The core-shell $MnCO_3$@MnO_2 microspheres were obtained when the solution transformed from purple to dark brown. After that, 80 mL of 1.2 mol/L HCl was added and the mixture solution was then stirred for 4 minutes followed by a rapid centrifuging process. After etched by HCl, the yolk structured $MnCO_3$(core)@MnO_2(shell) micro-spheres were obtained. The as-obtained powder was washed (with water and alcohol solution) for six times and dried at 80 °C for 1 hour in vacuum. Finally, the as-prepared yolk-structured $MnCO_3$(core)@MnO_2(shell) microsphere was further oxidized to pure yolk-structured MnO_2 microsphere by additional heat treatment (400 °C for 10 hours).

(3) Synthesis of yolk-structured $LiNi_{0.5}Mn_{1.5}O_4$ microspheres

The as-prepared yolk-structured MnO_2 microsphere was mixed and ground with lithium hydroxide mon-hydrate $(LiOH{\cdot}H_2O)_2$ and Nickel nitrate hexahydrate $(Ni(NO_3)_2{\cdot}H_2O)$ in the stoichiometric molar ratio (Li: Ni: Mn=1.05: 0.5: 1.5). Then the mixtures were calcined at 800 °C for 20 hours in air atmosphere.

The $LiNi_{0.6}Co_{0.2}Mn_{0.2}O_2$ and $LiNi_{0.8}Co_{0.1}Mn_{0.1}O_2$ (NCM-622 and NCM-811) cathode materials were provided by Prof An-Min Cao in Key Laboratory of Molecular Nanostructure and Nanotechnology, Beijing National Laboratory for Molecular Sciences, Institute of Chemistry, Chinese Academy of Sciences (CAS), Beijing, People's Republic of China. The $LiNi_{0.3}Co_{0.3}Mn_{0.3}O_2$ (NCM-333) was purchased from Amperex Technology Limited Company (ATL), China.

2.1.2 Electrolytes

$LiPF_6$-EC/DMC electrolyte was purchased from Wako Pure Chemical Industries Ltd. The pre-dried electrolyte was prepared by adding CaH_2 into the $LiPF_6$-EC/DMC electrolyte (none pre-dried) used in our glove box. Electrolytes with different water contents were prepared by adding corresponding amount of water into commercial $LiPF_6$-EC/DMC electrolyte (200, 500, 600 and 800 ppm defined as E-200, E-500, E-600 and E-800). The exact water concentrations in electrolytes were measured by Karl Fischer titration.

2.1.3 Synthesis of CuBTC MOF film as in-built water scavenger

(1) CuBTC was selected owing to its porous structure and excellent water adsorbing ability. Firstly, 0.24 g cupric nitrate trihydrate $(Cu(NO_3)_2{\cdot}3H_2O$, Sigma-Aldrich) was thoroughly dissolved in 25 mL ethanol and 0.105 g 1,3,5-Benzenetricarboxylic Acid (BTC, Sigma-Aldrich) thoroughly dissolved in 25

ml ethanol, respectively. The obtained two solutions were then thoroughly mixed together and followed by stirred for 2 hours. The obtained blue color CuBTC composite was then washed with water and ethanol for 6 times (each for 3 times). Next, the CuBTC composite was immersed into ethanol for 36 hours with ethanol solvent (Tokyo Chemical Industry (TCI)) replenished for 3 times to extrude water molecules confined inside CuBTC nano/subnano channels. After that, a centrifugation was also implemented to collect the final CuBTC composite. The harvested CuBTC composite was then initially dried at 80 °C for 12 hours followed by a final vacuumed dry process at 180 °C for 72 hours to generate the activated CuBTC powder sample.

(2) Fabrication of flexible CuBTC MOF film

The prepared activated CuBTC MOF powder was then employed to fabricate the flexible CuBTC MOF film as in-built water scavenger. Firstly, 90 wt. % activated MOFs samples were thoroughly mixing with 10 wt% polyvinylidene difluoride (PVDF, Tokyo Chemical Industry (TCI)) in dimethylformamide (DMF, Tokyo Chemical Industry (TCI)). After the CuBTC MOF slurries were obtained, we then uniformly spread them on the surface of Al foil followed by a primary drying procedure at 80 °C for 10 minutes. The Al foil covered by MOF film was then immersed into methanol solution for 5 minutes to facilitate the flexible CuBTC film detached from the Al foil. The obtained CuBTC MOF film was also submitted to undergo an activation process to extrude water molecules that possibly involved during the fabrication process. The prepared activated MOF film was then cutted into small plates (16 mm in diameter) and re-activated under vacuum at 180 °C overnight before transferred into glove box for cell assemble.

2.1.4 Electrodes Preparation

The prepared LNMO, NCM-333, NCM-622, NCM-811 and commercial lithium foil (Lion Chemical Industry Co., Ltd.) were used as electrode materials. Generally, 0.2 g electrode powders were stirring into a binder gel solution, which composed by carbon black, polyvinylidene fluoride (PVDF, Du Pont-Mitsui Fluorochemicals Co. Ltd.) powder (8:1:1) and N-methyl pyrrolidine (NMP, Sigma Aldrich, 99%) solvent (PVDF:NMP=6:94 wt%). The obtained slurry was then homogeneously coated onto Al foil current collector by a scraper. After tiny pressing procedure, the active materials-loaded metal foil was vacuum dried at 110 °C overnight, and final electrode plates (11 mm in diameter) were punched out. The mass loading of the cathode materials were about 3.0-3.2 mg/cm^2.

2.1.5 Cell Assembly and Electrochemical Measurements

CR2032 coin cells were assembled in an argon-filled glove box, in which both the moisture and oxygen contents were controlled to be less than 1 ppm. The normal (without pre-dried) electrolyte was 1 M $LiPF_6$-EC/DMC with a volume ratio of 1:1. Cathodes, Glass Fiber, MOF film and lithium anode were orderly placed into 2032 coin-type cells followed by adding electrolytes within different various water contents (50 μL for each cell). The cells were operated with a potential limit between: 3.0-4.9 V (for Li//LNMO cell) and 2.7-4.4 V (Li//NCM-333, Li//NCM-622 and Li//NCM-811 cell) in the study. Before each electrochemical characterization, the cells were kept on open circuit for 10 hours. All of the potentials in this study were referenced to Li/Li^+. For 2032 coin-type cells, the galvanostatic electrochemical measurements were carried out under potential control using the battery tester system HJ1001SD8 (Hokuto Denko) at 25 °C. Typically, the characterizations of the cell were carried out under galvanostatic control at the specific current density from the open-circuit

potential (OCP) unless other noted. For the EIS and CC-CV mode tests, the electrochemical experiments were carried out under the control of a potentiostat (Potentiostat/Galvanostat PGSTAT30, Autolab Co. Ltd., Netherlands) at room temperature. The current and potential outputs from the potentiostatic were recorded by a multifunction data acquisition module/amplifier (PGSTAT30 Differential Electrometer, Autolab), which was controlled by General Purpose Electrochemical Software (GPES). For the specific test conditions, we will show them in their corresponding sections in related supplementary figures.

2.1.6 Characterizations

(1) SEM, XRD and XPS Characterizations

The morphology of the as-prepared products was characterized with scanning electron microscopy (SEM, JEOL JSM-6380LV FE-SEM). X-ray photoelectron spectroscopy (XPS) was performed using a VG scientific ESCALAB 250 spectrometer with monochromic Al Kα excitation (1486.6 eV). X-ray diffraction (XRD) measurements were performed on a Bruker D8 Advanced diffractometer fitted with Cu-Kα X-rays (λ =1.5406Å) radiation at a scan rate of 0.016 °/s. For the pre-treatment procedures: The cycled cells were transferred into an Ar glove box once the electrochemical treatments were finished, and the electrodes were extracted from the cell and placed in a glass bottle. The electrode plates were twice rinsed by dimethoxyethane (DME, Sigma Aldrich, 99%) to wash off the electrolyte salt and the residual solvent, and then evaporated in a vacuum chamber, connected to the glove box, for 12 hours. The dried electrode plates were moved back to glove box and placed onto a SEM or XPS sample holder. The sample holder was sealed in an airtight container and then transferred into the SEM or XPS sample loading chamber. Note that, in order to restrain the exposure time to the ambient, samples (cycled electrode

plates) were tightly sealed into a glass bottle (fill with Ar gas), and transferred to the related chambers (SEM and XPS) as quickly as possible. Thus, we assumed the morphology and the component of electrode surface would not obviously change for such a short time exposure to the open air.

(2) Nuclear Magnetic Resonance (NMR) Spectroscopy Characterizations

The NMR spectra were recorded using a spectrophotometer (500 MHz Ultra-ShieldTM, Bruker). Typically, 256/128 ($^{1}H/^{19}F$) times were accumulated for one spectrum. The electrodes and separators were extracted from the cycled cells without further pretreatment. 750 μL of D_2O (99.9 atom % D, Wako Chemicals) was used to extract the residual electrolyte and soluble parasitic products (mainly carboxylates and fluorides) from the electrodes and the separators, then the solution was transferred to septa-sealed NMR tube. To quantify the amount of related components, 1 μL of benzene (C_6H_6, Sigma Aldrich, 99%) and 1 μL of fluorobenzene (C_6H_5F, Sigma Aldrich, 99%) were mixed and injected through the septa and employed as an internal standard. The method here was very similar as the ones introduced in our previous works.

(3) Inductively-Coupled Plasma (ICP) Characterizations

ICP-OES (optical emission spectroscopy) results were recorded using Thermo Scientific iCAP 5600 and PerkinElmer Optima 4300 DV. Metal dissolutions from the LNMO, NCM-622-based electrodes were quantitatively confirmed measuring the Mn and Ni-ion concentrations both in the electrolyte solutions and on the lithium-metal anode. The cycled separators (infiltrated by cycled electrolyte solutions) and lithium electrodes were bathed in DME solvent for 4 hours aging. The separator was salvaged out then the DME solution and Li anode were mixed with a mixture of concentrated hydrochloric acid and nitric acid mixture (3:1 in volume ratio). The solution was heated in a microwave for 2 hours (150 °C).

2.1.7 Highlights of Chapter 3

As discussed in chapter 1, the electrolyte related decomposition problems greatly influence the electrochemical performance of lithium-metal batteries (LMBs), especially the high-voltage LMBs. Water molecules contained and formed inside cells can largely deteriorated the whole battery system and consequently cause transition metal dissolution, cathode/anode degradation and electrolyte decomposition. By using CuBTC MOF as in-built water scavengers can effectively suppress these aforementioned detrimental issues. Through using multiple physical and chemical characterization technologies, we demonstrated significantly suppressed water induced HF-related side reactions. Benefit from the excellent water extruding properties of the prepared CuBTC MOF based in-built water scavenger, inspiring high-voltage LMBs can be achieved even under harsh environment (200-500 ppm water containing electrolyte under 55 ^{o}C). The improved results can also be found under high cathode mass loading (about 10 mg/cm^2). The finding of using MOF to suppress water induced HF-related detrimental issues could greatly reduce the costs and energy consumed during the purification of electrolytes and the fabrication of cells.

2.2 Experimental section of Chapter 4

2.2.1 Preparation of different MOF composites

2.2.1.1 Preparation of the modified MOF composites:

(1) Synthesis of copper hydroxide nanorods (CHNs): Cupper hydroxide nanostrands (CHNs) were firstly synthesized by quickly mixing equal volume 1.16 g copper nitrate hexahydrate solution (300 ml) with 100 mg aminoethanol aqueous solution (300 ml) at room temperature and aged for 48 h. The CHNs composites were

collected by filtering the mixture onto an organic membrane. Then, the Ms-9.0 was successfully obtained by immersing the CHNs film into 10 mM BTC water-ethanol (water/ethanol volume ratio 1:1, 40 ml) solution at room temperature for 12 h. The obtained composite was finally vacuumed at 180 °C for 72 h to generate the activated MOF sample.

(2) Synthesis of modified MOF (CuBTC-NSP):

After the CHNs were obtained, 12 mg NSP was added into 300 ml CHNs solution to prepare the CHNs-NSP composites. Then the Ms-9.0-NSP was prepared as same as that in the preparation process in Ms-9.0 from CHNs. The obtained modified MOF was finally vacuumed at 180 °C for 72 h to prepare the activated modified MOF sample.

2.2.1.2 Preparation of MOF film

MOF based solution was prepared by thoroughly mixing 90 wt. % activated MOF sample with 10 wt% Polytetrafluoroethylene (PTFE) in ethanol. The obtained MOF slurries were then quickly stirred to mix the sample evenly and evaporate the unnecessary organic solvent, finally resulting in sticky MOF putty. The obtained MOF putty was then uniformly spread on the Al foil and then dried at 80 °C for 10 min in drying oven. The MOF coated Al foil was then immersed into methanol for 5 min until the MOF film was detached from the Al foil and formed the flexible MOF film. The MOF film was then further compacted more than 10 tons of pressure to remove the inter-particle pores. The obtained MOF film was firstly dried at 80 °C for 1 hour in drying oven and then followed by vacuumed dried oven at 180 °C overnight to activate the MOF film. The prepared activated MOF film was then cutted into small plates (16 mm in diameter) and re-activated under vacuum at 180 °C overnight before transferred into glove box for further usage.

2.2.2 Preparation of carbonate electrolyte.

Before this process, carbonate electrolytes (PC-LiTFSI) with different concentrations (1M and 3M) were firstly prepared. Typically, for the preparation of 1M PC-LiTFSI carbonate electrolyte, 2.87 g LiTFSI salt was mixed with 10 mL Propylene Carbonate (PC) solvent and stirred at 60 °C for 2 hours. 3M carbonate electrolytes were prepared follow the same procedures except stoichiometric LiTFSI salt was added.

2.2.3 Preparation of the over-saturated carbonate electrolyte (PC-LiTFSI with MOF).

The afore prepared activated MOF small plates were immersed into the 1M PC-LiTFSI electrolyte under 90 °C for 48 hours to soak electrolyte molecules into MOF channels. Then, the MOF plates filled with electrolyte were taken out, wiped with tissues followed by a physical press step and dried under a vacuum for 24 hours at 80 °C to get rid of any possible electrolyte solvents on the surface.

2.2.4 Synthesis of the 5.3 V-class $LiCoMnO_4$ composites

Firstly, 4.2 mmol $CoCl_2 \cdot 6H_2O$ and 3.5 mmol $MnCl_2 \cdot 4H_2O$ was dissolved in 132 mL of distilled water, and 4.9 g of urea, 5.0 g of ascorbic acid, and 4.0 g of polyvinylpyrrolidone (molecular weight 40K) were then added to the $CoCl_2/MnCl_2$ solution in sequence under stirring for 1 hour. After being stirred for 1 hour, the solution was transferred to a 100 mL Teflon-lined stainless-steel autoclave and maintained at 160 °C for 6 hours. The $CoMnCO_3$ microspheres were obtained after being centrifuged, washed with water and ethanol several times, and dried at 60 °C overnight. The obtained $CoMnCO_3$ microspheres were calcinated in air at 400C for 5 hours to obtain the $CoMnO_x$ microspheres. Then, 0.700 g of $CoMnO_x$ and 0.165 g of

Li_2CO_3 were mixed and calcinated at 800 °C for 24 hours in an O_2 atmosphere to obtain the $LiCoMnO_4$ product. The synthesis process can also be simplified as follow: In fact, the $LiCoMnO_4$ in this manuscript can be obtained followed by mixing $MnCO_3$, Co_3O_4 and Li_2CO_3 precursors under a certain ratio. Specifically, the stoichiometric ratio among the three composites can be simplified as the ratio of Li: Co: Mn elements. The ratio of Li: Co: Mn was 1.1: 1: 1. After a calcination process, the final 5.3 V-class $LiCoMnO_4$ can be obtained.

2.2.5 Electrodes Preparation

The obtained $LiNi_{0.8}Co_{0.1}Mn_{0.1}O_2$ (defined as NCM-811, provided by Prof An-Min Cao from Chinese Academy of Sciences (CAS)), the synthesized $LiCoMnO_4$ (defined as LCMO) and lithium foil (Lion Chemical Industry Co., Ltd.) were employed as electrode materials. Generally, 1.0 g electrode powders mixed with carbon black and polyvinylidene fluoride (PVDF, Du Pont-Mitsui Fluorochemicals Co. Ltd.) powder in a ratio of 8:1:1 and then directly stirring for 4 hours to get a viscous solution. The obtained slurry was then homogeneously coated onto Al foil current collector by a scraper. After tiny pressing procedure, the active materials-loaded Al foil was vacuum dried at 110 °C overnight. Part of the obtained cathode was cutted into final electrode plates (11 mm in diameter), and the mass loading of the NCM-811 and LCMO cathode materials were about 9.2-9.4 mg/cm^2 for full cells with one time excess Li. For cells cycled under harsh practical condition, around 18.4-18.9 mg/cm^2 of cathode materials were coated and tested with ultra-thin Li anode (about 37.2 and 60 μm).

2.2.6 Cell Assembly and Electrochemical Measurements

CR2032 coin cells were assembled in an argon-filled glove box, in which both

the moisture and oxygen contents were controlled to be less than 1 ppm. The prepared solvent-depleted carbonate electrolyte (PC-LiTFSI with MOF) was closely attached to the high-voltage cathodes and followed by a physical pressing process. The obtained cathode & electrolyte was then physically pressed on the surface of Li anode and then placed in the coin cell for cell assembling. For comparisons, cells using conventional carbonate electrolytes (1M PC-LiTFSI without MOF, 70 μL) were also assembled accompanied with the glass fiber as separators. The NCM-811//Li cells were operated with a potential limit between: 2.7-4.4 V in the study. The LCMO//Li cells were cycled between 3.0-5.3 V in this paper. Before each electrochemical characterization, the cells were kept on open circuit for 10 hours. All of the potentials in this study were referenced to Li/Li^+. For 2032 coin-type cells, the galvanostatic electrochemical measurements were carried out under potential control using the battery tester system HJ1001SD8 (Hokuto Denko) at 25 °C. For the Linear sweep voltammetry (LSV), PITT, EIS and CV tests, the electrochemical experiments were carried out under the control of a potentiostat (Potentiostat/Galvanostat PGSTAT30, Autolab Co. Ltd., Netherlands) at room temperature. The current and potential outputs from the potentiostat were recorded by a multifunction data acquisition module/amplifier (PGSTAT30 Differential Electrometer, Autolab), which was controlled by General Purpose Electrochemical Software (GPES). For the specific test conditions, we will show them in their corresponding sections in related supplementary figures.

2.2.7 Morphology and Structure Characterization

2.2.7.1 SEM, XRD, TEM and XPS Characterizations

The morphology of the as-prepared MOF products, pristine cathodes and cycled cathodes and Li anodes were characterized with scanning electron microscopy (SEM, JEOL JSM-6380LV FE-SEM). Moreover, the cycled NCM-811 and LNMO cathodes

were also characterized with transmission electron microscopy (TEM, Tecnai G2 F30 S-TWIN). X-ray photoelectron spectroscopy (XPS) was performed using a VG scientific ESCALAB 250 spectrometer with monochromic Al Kα excitation (1486.6 eV). X-ray diffraction (XRD) measurements were performed on a Bruker D8 Advanced diffractometer fitted with Cu-Kα X-rays (λ =1.5406Å) radiation at a scan rate of 0.016 °/s. For the pre-treatment procedures: The cycled cells were transferred into an Ar glove box once the electrochemical treatments were finished, and the electrodes were extracted from the cell and placed in a glass bottle. The electrode plates were twice rinsed by dimethoxyethane (DME, Sigma Aldrich, 99%) to wash off the electrolyte salt and the residual solvent, and then evaporated in a vacuum chamber, connected to the glove box, for 12 hours. The dried electrode plates were moved back to glove box and placed onto a SEM or XPS sample holder. The sample holder was sealed in an airtight container and then transferred into the SEM or XPS sample loading chamber. Note that, in order to restrain the exposure time to the ambient, samples (cycled electrode plates) were tightly sealed into a glass bottle (fill with Ar gas), and transferred to the related chambers (SEM and XPS) as quickly as possible. Thus, we assumed the morphology and the component of electrode surface would not obviously change for such a short time exposure to the open air.

2.2.7.2 Nuclear Magnetic Resonance (NMR) Spectroscopy Characterizations

The NMR spectra were recorded using a spectrophotometer (500 MHz Ultra-ShieldTM, Bruker). Typically, 256/128 ($^{1}H/^{19}F$) times were accumulated for one spectrum. The electrodes and separators were extracted from the cycled cells without further pretreatment. 750 μL of D_2O (99.9 atom % D, Wako Chemicals) was used to extract the residual electrolyte and soluble parasitic products (mainly carboxylates and fluorides) from the electrodes and the separators, then the solution was transferred to septa-sealed NMR tube. To quantify the amount of related

components, 1 μL of benzene (C_6H_6, Sigma Aldrich, 99%) and 1 μL of fluorobenzene (C_6H_5F, Sigma Aldrich, 99%) were mixed and injected through the septa and employed as an internal standard. The method here was very similar as the ones introduced in our previous works.

2.2.7.3 Spatial resolution Operando-Raman Spectroscopy Characterizations

The Raman spectra were recorded using a JASCO microscope spectrometer (NRS-1000DT). The spectral resolution of the Raman spectra in the study was ca. 1.0 cm^{-1}. Typically, the scattering signal in Raman spectrum was weak and hard to be investigated. In this case, in order to obtain strong and clear peaks on the spectra, we took advantage of a shell-isolated nanoparticle-enhanced Raman spectroscopy (SHINERS) technique that evidently enhances the scattering signal.[S5] Briefly, Au nanoparticles (NPs) were synthesized with a diameter of 30~40 nm as core by a standard sodium citrate reduction method. Then freshly prepared aqueous solution of 1 mM (3-aminopropyl) trimethoxysilane (APS, Sigma Aldrich) was added to the gold sol under vigorous magnetic stirring for 15 minutes, followed by the addition of a 0.54 wt % sodium silicate solution (Tokyo Chemical Industry Co., Ltd). Then, the solution was heated to 90 °C under vigorous magnetic stirring for 1 hour. The series of steps ensures the formation of an ultra-thin SiO_2 shell (2-4 nm) without any pinhole. The washed and dried Au@SiO_2 NPs were re-dispersed in ethyl alcohol. Finally, the obtained Au NPs solution was mixed with MOF particles together with NMP as solvent before the NPs contained MOF was coated on the surface of NCM-811 cathode for Raman experiment. These Raman samples were further dried in vacuum at 80 °C for 18 hours before assembled into the cell. Note that the amount of deposited NPs was very small, so that we assumed it would not cause any influence on the electrochemical behaviors.

2.2.8 FT-IR Characterizations

2.2.8.1 Fourier-transform infrared (FTIR) Characterizations

FTIR measurements were carried out on a FT/IR-6200 spectrometer (JASCO Corp.). Typically, 64 interferograms were accumulated for one spectrum with a resolution of 4.0 cm^{-1}. For pretreatment, the cycled cells were transferred into an Ar glove box once the discharge finished, and the cathodes were extracted from the cell and twice rinsed by dimethoxyethane (DME, Sigma Aldrich, 99%) to wash off the electrolyte salt and the residual solvent, and then evaporated in a vacuum chamber, connected to the glove box, for ~15 min. The dried cathode was scratched off (nearly 1×2 mm^2) and then grounded together with potassium bromide (KBr, FTIR grade, purity of >99 %, Sigma Aldrich). The KBr powder was dried in vacuum at 100 °C for 24 hours before using, and the grinding procedure was carried out in an Ar-filled glove box. The mixture powder was pressed into hyaline pellets in vacuum under high pressure (4.0 Mpa) for 5 minutes. For the characterization of electrolyte solution, the cycled electrolyte was uniformly coated onto the KBr pellet in Ar-filled glove box. The KBr-based pellet was sealed in an airtight container and then rapidly transferred into the IR sample loading chamber, in which continuously purged with inert argon gas. The composites were tested using the common FT-IR following the aforementioned experiment procedures

2.2.8.2 Etching Fourier-transform infrared (FTIR) Characterization

For pretreatment, the cycled cells were transferred into an Ar glove box once the discharge finished, and the cathodes were extracted from the cell and twice rinsed by dimethoxyethane (DME, Sigma Aldrich, 99%) to wash off the electrolyte salt and the residual solvent, and then evaporated in a vacuum chamber, connected to the glove box, for ~15 min. For the etching-FTIR experiment, the measurements were carried out on IRT-5200 Infrared Microscope spectrometer (JASCO Corp.) with PR0450-S

attenuated total reflection (ATR) accessories. Typically, 64 interferograms were accumulated for one spectrum with a resolution of 4.0 cm^{-1}. For the etching process, the cycled electrode plate was assembled onto the sputtering target within an auto fine coater (JFC-1200, JEOL) in a vacuum environment (10~20 Pa, 10~15 mA current). The etching time was fixed at 10 s per time. The cycled NCM-811 cathode used over-saturated carbonate electrolyte (1 M PC-LiTFSI with MOF) and the cycled NCM-811 cathode used common carbonate electrolyte (1 M PC-LiTFSI without MOF) were tested using the etching FT-IR following the aforementioned experiment processes.

2.2.9 Highlights of Chapter 4

As mentioned in chapter 1, the serious electrolyte decompositions severely hindered the development of LMBs, especially the high-energy-density LMBs. However, both conventional ether-based electrolytes and carbonate-based electrolytes have their corresponding drawbacks, thus prevent them been used for high-voltage LMBs. By confining electrolyte inside MOF channels, a unique over-saturated carbonate electrolyte with special over-saturated configuration was designed. The rational designed over-saturated electrolyte make it compatible with both oxidative high-voltage cathodes and reductive Li-metal anodes (enlarged the stability window from 4.5 V to 5.4 V, and much stable lithium reversibility). Variable techniques (scanning electron microscopy (SEM), galvanostatic intermittent titration technique (GITT), Raman spectra, etching FT-IR and NMR etc.) are employed to analyze the characteristics of the prepared over-saturated electrolyte. Largely enhanced electrochemical performance of high-energy-density LMBs (NCM811//Li, LCMO//Li) were finally achieved. We anticipate that the finding will remedy the inherent defects of conventional liquid electrolytes and push the development of high-energy-density

LMBs into practical commercial applications.

Chapter 3. MOF based in-built water scavenger addresses detrimental issues induced by water existed in carbonate electrolyte for high-voltage lithium-metal battery

3.1 Introduction.

Lithium-metal batteries (LMBs) have attracted tremendous attention due to their potential in providing higher energy density compared to conventional lithium-ion batteries (LIBs).[15, 28, 29, 54-56] For rechargeable LMBs, various detrimental issues (e.g. hydrolysis of electrolytes, accumulation of HF, transition metal dissolution and Li corrosions) induced by water on both cathodes and anodes has been ignored.[37-39] Therefore, aiming to improving the battery performance, a lot of efforts have been made to address these annoying problems induced by water in electrolytes.[39] Yet, no specific effective methods have been proposed to permanently solve this annoying problem so far due to the intrinsic drawbacks of conventional water removing strategies: (1) the unsustainable water removal effects and (2) the insufficient water removal effectiveness: since traditional water removal methods are using rigid one-time pre-treatment of drying electrolytes and expensive dry-room for cell fabrications, only water already existed in electrolytes are expected to be removed while the subsequent continuously accumulated water upon cell fabrication and electrochemical cycling cannot be extruded. Hence, it is highly important to find an effective method to solve this tricky problem and consequently enhance the electrochemical performance of LMBs.

Recently, due to their special high surface areas and various nano/subnano pores, metal-organic frameworks (MOFs) were extensively employed as molecular scavengers for gas separations.[57-61] Very recently, MOFs have also been used as

water-collector to capturing water existed in the air.[62-64] Also, MOFs were reported can functionalized efficiently as interlayers and protective layers in LMB systems.[65-71] This implies MOFs own the possibility and potential of becoming promising efficient and continuous in-built water scavenger for LIBs.[61, 72] Herein, we focus on the representative MOF ($Cu_3(BTC)_2$) and investigate its water scavenging ability and the corresponding influences in high-voltage LMBs by using XPS, ICP, NMR analysis and electrochemical tests.

We demonstrated that the existence of water in LMBs could trigger severer transition metal dissolutions (TM loss). This in-built water scavenger can not only scavenge water already (in electrolytes, electrodes and separators) within cells, but also adsorb water accumulated upon electrochemical cycling constantly, which is an unprecedented achievement that none traditional methods/procedures can reach. By using MOF based in-built water scavenger, the electrochemical performance of typical high-voltage LMBs (LNMO//Li, NCM811//Li) were apparently enhanced compared with that without using MOF based in-built water scavenger. ICP, XPS, NMR and XRD together verified that the typical detrimental water-related side reactions like hydrolysis of electrolytes, accumulation of HF, transition metal dissolution and Li corrosions were significantly suppressed after MOF based in-built water scavenger was employed. This method is an unprecedented achievement that none traditional methods/procedures can reach.

3.2 Negative effects of water exist in lithium-metal battery

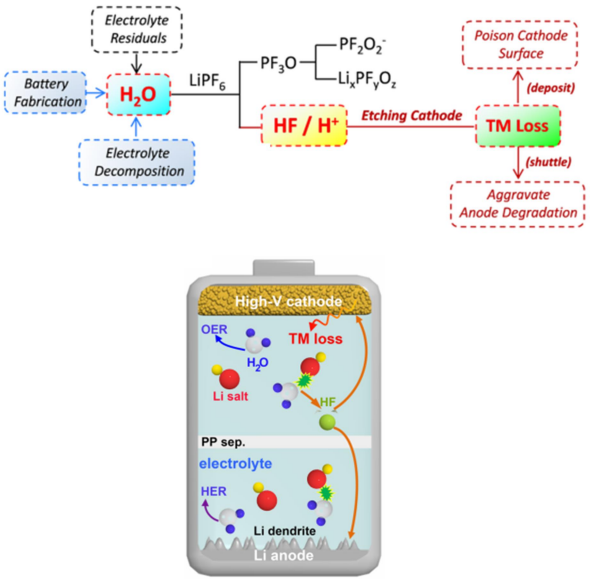

Figure 3. 1 Negative effects of water exist in lithium-ion battery. (a) Proposed mechanism of the different sources of and the corresponding negative effects of water contained in lithium ion batteries (LIBs). (b) Graphical representation of the negative influences of water in accelerating transition metal dissolution (TM loss), arising hydrogen evolution reaction (HER) and oxygen evolution reaction (OER), and degrading lithium anode.

As discussed in Chapter 1, even considerable progresses related to high-voltage lithium metal batteries (LMBs) have been reported in recent years, the electrochemical performances however, still been restricted by the annoying detrimental transition metal dissolutions induced by attacked by HF, induced by water existed in LMBs as shown in **Figure 3.1**. In addition, owing to the same reason, serious hydrogen evolution reaction (HER) and oxygen evolution reaction (OER) would happen, which will consequently form various gaseous finally products and lead to potential safety hazards.[37] Moreover, fast lithium-metal degradation can also be found after several electrochemical cycles. Those detrimental phenomena can be ascribed to the appearance of water molecules in LMBs. To fully extrude water from

cells, it is important to clearly figure out the different sources that can bring/produce water inside LMBs.[39] As demonstrated in **Figure 3.1**, there are three different processes that can bring and/or produce water into/inside LMBs. Despite water contained in electrolytes (electrolyte residuals), water can also be accumulated and produced during cell fabrication and electrolyte decomposition during electrolyte cycling. Since traditional water removal methods are using rigid one-time pre-treatment of drying electrolytes and expensive dry-room for cell fabrications, only water already existed in electrolytes are expected to be removed while the subsequent continuously accumulated water upon cell fabrication and electrochemical cycling cannot be extruded. Water from these two sources can deteriorate the cell performances.

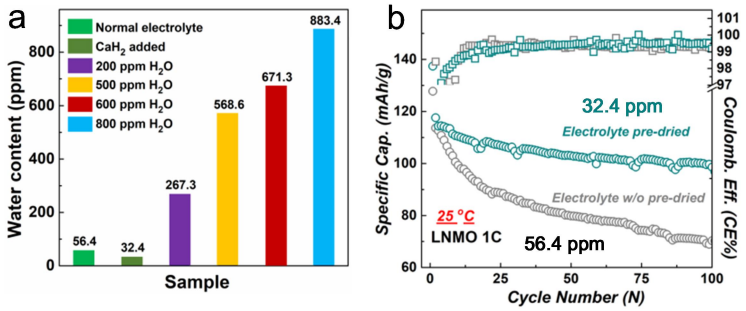

Figure 3. 2 (a) Accurate water contents contained in different electrolytes. (b) Electrochemical performances of the Celgard separator based Li//$LiNi_{0.5}Mn_{1.5}O_4$ (LNMO) cells. (a) Cycling performances of the LNMO cells cycled in commercial electrolyte without (w/o) pre-dried (grey trace) and pre-dried electrolyte (dark green trace) at 1 C current rate in room temperature of 25 ^{o}C.

As can be found in **Figure 3.2a**, when CaH_2 as water-drier was added into the commercial carbonate electrolytes ($LiPF_6$-EC/DEC), the water content was sharply dropped from 56.4 (electrolyte without drying) to 32.4 ppm (pre-dried electrolyte). These two electrolytes were then coupled with $LiNi_{0.5}Mn_{1.5}O_4$, Celgard separator and lithium to fabricate Li//$LiNi_{0.5}Mn_{1.5}O_4$ (LNMO) cells. As clearly shown in **Figure**

3.2b, when cycled under current rate of 1 C (147 mA g^{-1}), the LNMO cell using pre-dried electrolyte demonstrated much better electrochemical performance than that of the LNMO cell assembled with un-dried electrolyte.

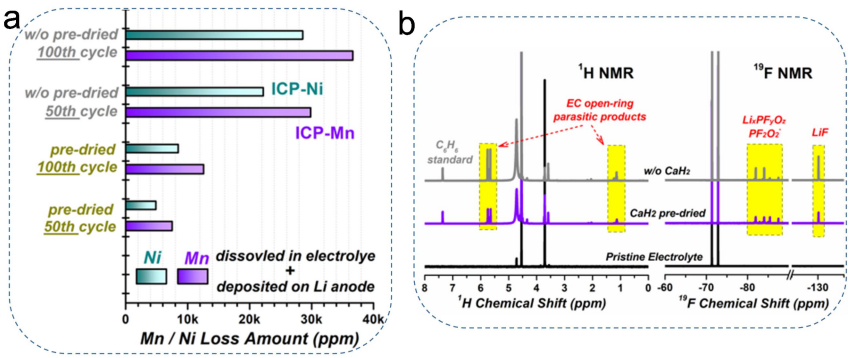

Figure 3. 3 (a) The ICP analysis results of Ni and Mn elements and (b) ^{1}H (left) and ^{19}F NMR (right) analysis of two cycled Li//$LiNi_{0.5}Mn_{1.5}O_2$ cells (using un-dried electrolyte: 56.4 ppm water and pre-dried electrolyte: 32.4 ppm water).

Moreover, Inductively-Coupled Plasma (ICP) and Nuclear Magnetic Resonance (NMR) Spectroscopy were also employed to verify the amount of TM loss and electrolyte decomposition products in two cells. Apparently, compared with the cell used un-dried electrolyte, the pre-dried electrolyte used cell demonstrated much relived Ni and Mn dissolution (dissolved in electrolyte and deposited on Li anode) after both 50^{th} and 100^{th} cycles. NMR also exhibited the similar results: The EC open-ring parasitic products and the formation of LiF can be clearly observed in LNMO cell using commercial electrolyte without pre-dried, while that of the electrolyte extracted from LNMO cell using pre-dried electrolyte shown alleviated electrolyte decomposition parasitic products and accumulation of HF-related side reaction products. The water contents in two cells, regarded as the only variable factor, were considered the reason lead to faster capacity decay, severer TM loss and electrolyte decomposition. This highlighted the importance of extruding water in LMBs.

3.3 Excellent water scavenging ability of the CuBTC MOF composites

As discussed before, due to the inherent defects of traditional water removal methods, a much efficient and simple which can enable continuous in-situ water removal effects during cell electrochemical cycling are highly desired for LMBs. So, we start to find out materials with excellent water adsorbing abilities in order to fulfill this goal. Due to their high specific surface areas and pore-rich nano/sub-nano structures, metal-organic frameworks (MOFs) were frequently studied during this past decades after they were discovered.[57, 73-77] For example, MOFs were employed as highly-efficient molecular sieves to adsorb gases and/or separate gases.[57, 58, 78-81] In recent few years, those porous MOFs materials were also been used as water scavengers to collect water from the atmosphere.[62, 63, 82, 83] Although inspiring results can be obtained by using various MOFs materials in those aforementioned fields, to fulfill the ultimate goal of scavenging water molecules existed in lithium-ion batteries/lithium-metal batteries (LIBs/LMBs), only MOFs which are chemical/electrochemical stable in (LIBs/LMBs) are expected to function as the potential candidates.[66, 70, 71] Very recently, several different MOFs were reported to be used as ion sieves, artificial protective layers and quasi-solid electrolytes and demonstrated enhanced electrochemical performances in LIBs/LMBs.[65, 84-86] Those results verify the excellent chemical/electrochemical stabilities of specific MOFs after used in LIBs/LMBs systems.[85, 87] Encouraged by those inspiring results, MOFs possess the possibility and potential to be used as efficient and continuous water scavenger for LIBs/LMBs.

Next step would be how to choose proper MOF to act as water scavengers. A typical MOF (CuBTC: $Cu_3(BTC)_2$, known as HKUST-1)[70, 88, 89] was chosen as water

scavenger in this work due to its microporous structure as shown in **Figure 3.4a**. We hope the unique structure of CuBTC MOF can promote reversible water adsorption and desorption. The absence and reappearance of the (111) peak of the CuBTC under different circumstances (the pristine CuBTC MOF, activated CuBTC and the activated CuBTC within further re-adsorb water) shown in the X-ray diffraction (XRD) pattern suggested the reversible water adsorption and desorption.[66, 90] This characteristic makes it essential different from conventional one-time self-destructive water removal additives (like Al_2O_3, CaH_2, etc.). To initially quantify the water adsorbing ability of the CuBTC MOF powder, thermogravimetric analysis (TG) of MOF samples were tested (**Figure 3.4b**). Apparently, even after pre-dried under vacuum at 100 °C for 12 hours, the activated CuBTC powder demonstrated 8.1 wt% weight losses which can be ascribed to the water confined inside MOF channels.

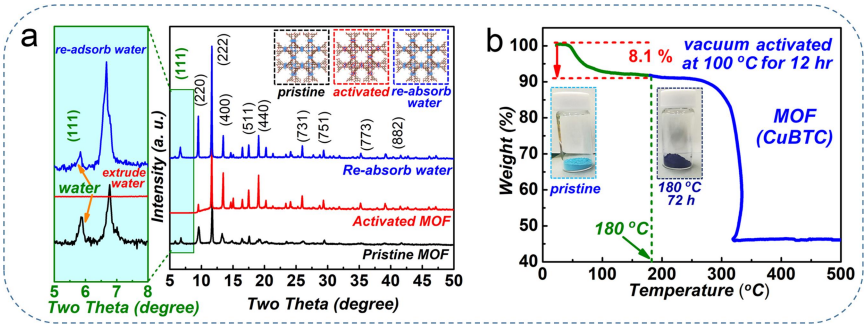

Figure 3. 4 (a) XRD results of the pristine CuBTC MOF powder-composite, the activated CuBTC MOF powder-composite and the activated MOF powder-composite after further re-adsorb water process. (b) And the corresponding TG curve of the MOF powders vacuum activated at 100 °C for 12 hours. The inset digital photos are taken form the pristine CuBTC MOF powder-composite dried in air at 60 °C for 6 hours (left) and the activated MOF vacuum dried at 180 °C for 72 hours (right).

To test its accurate water adsorbing value, CuBTC MOF powders (50 mg for each time) were then added into the same amount of electrolytes (1 mL) that contained different amount of water (100, 200 and 500 ppm) before measured by Karl

Fischer titration. Apparently, after 48 hours immersion, electrolytes with addition of MOF powers all experienced dramatic drop in water contents and finally maintained at a much lower water levels than that pre-dried by CaH_2 (as shown in **Figure 3.2a**).

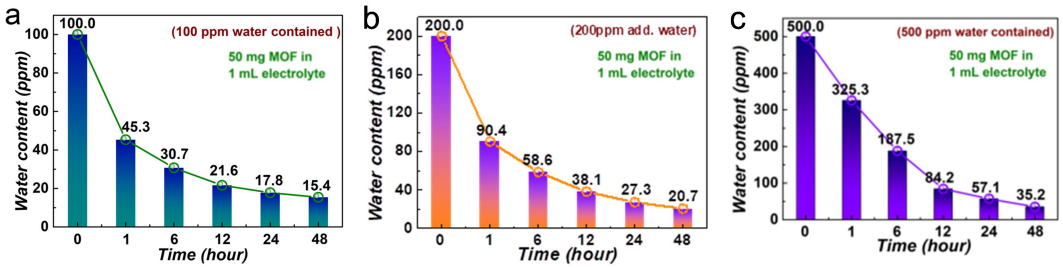

Figure 3. 5 Testing the water adsorption ability of the obtained activated MOF powder after adding 50 mg MOF powder into 1 mL electrolytes containing (a) 100 ppm and (b) 500 ppm water.

Noted that owing to their powder-like feature, MOF powders cannot be directly added into batteries and used water scavengers. We then mixed the activated CuBTC MOF powder with polymer binder to fabricate a flexible CuBTC MOF film,[88, 91-93] which was consequently functionalized as in-built water scavengers for LMBs during electrochemical cycling processes (**Figure 3.6a** and **b**). As shown in **Figure 3.6c** and **d**, the prepared CuBTC MOF film demonstrated excellent flexibility even after been bended seriously (inset in **Figure 3.6c**). A further de-gas procedure was also implemented aiming to remove moisture before send these obtained CuBTC MOF films (cutted into small plates with 16 mm in diameter, 5 mg mass loading for each piece) into glove box.[94]

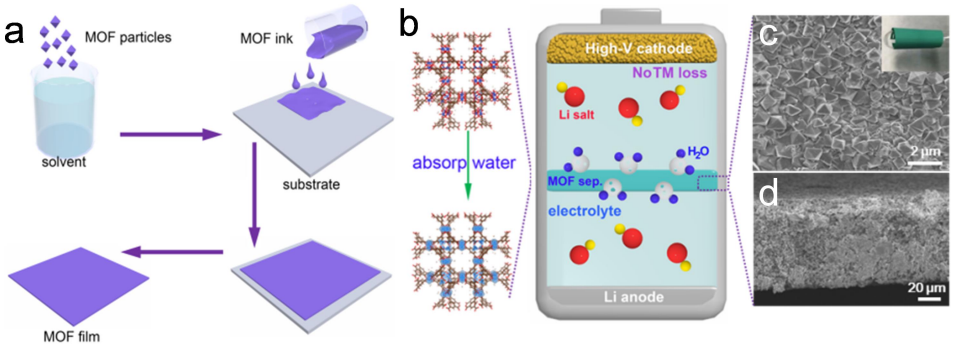

Figure 3. 6 (a) The preparation of the MOF separator. (b) Schematic illustration of the significant role of water restraining MOF for electrolyte in LMBs. (c and d) Digital photo and the corresponding SEM images of the obtained MOF separator.

Since excellent result can be obtained after 50 mg MOF powder was immersed into 1 mL 1000 ppm water contained electrolyte as shown in **Figure 3.7a**, considered the mass loading of one piece MOF film (5 mg/piece), one piece of MOF film calculated can maximally adsorb 0.03712 mg water which even slightly higher than water contained in 600 ppm water added electrolyte (**Figure 3.7b**). This indicates that CuBTC MOF film holds promising potential to scavenge water in LIBs/LMBs.

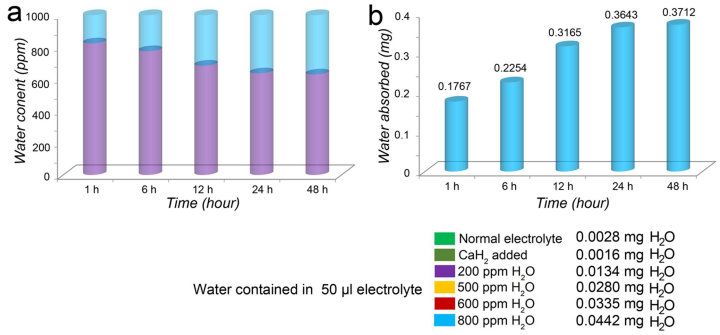

Figure 3. 7 (a) 50 mg MOF powder immersed into 1 mL 1000 ppm water contained electrolyte to probe the amount of the remained water. (b) The corresponding calculated water adsorption ability of 50 mg MOF powder and the accurate water contents in different electrolytes (50 μL for each cell) used in fabricating coin cells.

3.4 Mechanism Analysis on MOF based in-built water scavenger suppress the detrimental effects induced by water

Typical high-voltage lithium-metal batteries (Li//$LiNi_{0.5}Mn_{1.5}O_4$; defined as LNMO) were assembled with MOF films based in-built water scavenger to investigate their water scavenging property. As can be found in **Figure 3.8a**, when both of the two LNMO cells cycled in commercial electrolyte without pre-drying, the MOF film assembled cell (blue curve) delivered much better cycling stability and Coulombic efficient (CE) than the Celgard separator used cell (light grey curve). To be more specific, the MOF film assembled cell delivered an initial capacity of 121 mAh g^{-1} (calculated from the 2nd cycle since the 1st cycle was activated at 0.1 C) and stabilized at 85 mAh g^{-1} after 500 cycles (corresponding to a slow capacity decay of 0.06% per cycle).

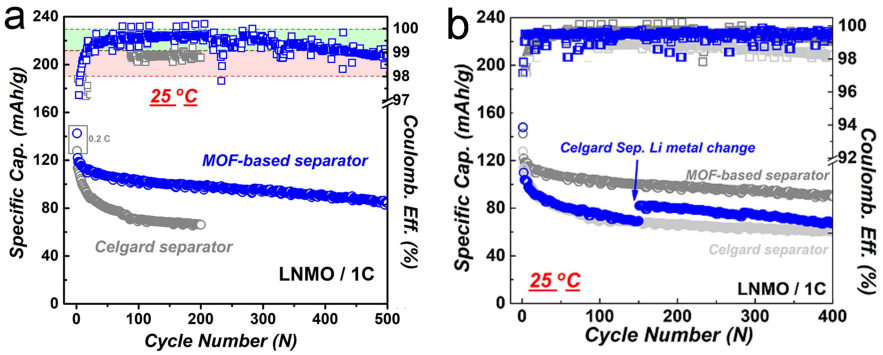

Figure 3. 8 (a) Cycling performances and corresponding coulombic efficiency (CE) of the LNMO cells assembled with Celgard separator and MOF based in-built water scavenger in commercial electrolyte (56.4 ppm water contained) at 1 C current rate. (b) And the Cycling performances and corresponding coulombic efficiency (CE) of the LNMO cells assembled with Celgard separator in commercial electrolyte (56.4 ppm water contained) at 1 C current rate with fresh Li anode be replaced after 150 cycles.

We also found that the Li anode degradation can lead to the decay of capacity for the LNMO cell used Celgard separator. As shown in **Figure 3.8b**, an apparent

capacity improvement can be observed when the Celgard separator based LMNO cell were replaced with fresh Li anode, compared with that of the LNMO cell which did not replace Li. The improvement was also verified by the much higher CE of the MOF used in-built water scavenger used LNMO cell. The mechanism of how the MOF based in-built water scavenger suppress the detrimental effects induced by water was under further investigation.

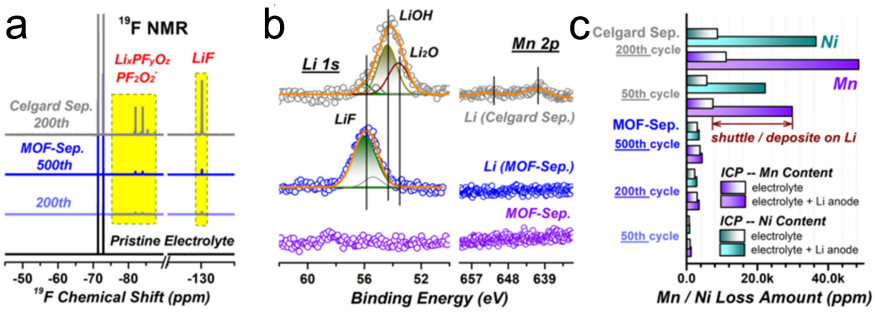

Figure 3. 9 (a) ^{19}F NMR analysis results of cycled electrolytes from two cells using Celgard separator and MOF based in-built water scavenger after different cycles. (b) XPS spectra of the cycled Li anodes harvested from LNMO cells assembled with Celgard and MOF separators in Li 1s (left) and Mn 2p (right) regions. (c) The corresponding ICP analysis (Ni, Mn) results of the two cycled LNMO cells assembled with Celgard separator and MOF based in-built water scavenger.

Both of the two cells were submitted to Nuclear Magnetic Resonance (NMR), X-ray photoelectron spectroscopy (XPS) and inductively coupled plasma (ICP) measurements for deeper analyses (LNMO cathodes, electrolytes, separators and Li anodes) as shown in **Figure 3.9** to prove the advantages of MOF based in-built water scavenger. As can be observed in **Figure 3.9a** (Nuclear Magnetic Resonance (NMR) spectra of ^{19}F), compared with electrolyte harvested from Celgard separator based LNMO cell, electrolyte collected from MOF used cell exhibits only trace of LiF and fluoride parasitic products. This indicates that water-related HF induced severer electrochemical decomposition was greatly suppressed through using MOF based

in-built water scavenger. The cycled Li anodes were also under further investigation to quantify the accumulation of decomposition products and dissolved metal-ions by using X-ray photoelectron spectroscopy (XPS). For the cell assembled with Celgard separator, we can found obvious MnF_x (**Figure 3.9b**, right, grey curve) deposited on the surface of cycled Li anode.[38] This part of Mn element can be ascribed to the serious shuttling and re-deposition of dissolved Mn from the LNMO cathode side. For sharp contrast, the cycled Li from the MOF in-built water scavenger based cell, inspiringly, demonstrated only trace of Mn deposition. In addition, the Li 1s spectra of the Celgard separator used Li exhibits severer accumulation of Li_2O, LiOH and LiF, while the MOF used Li anode demonstrated only the formation of LiF.[38] This suggests the apparently suppressed water related Li anode degradation in MOF based in-built water scavenger used cell, which can also be verified by the cycling performance shown in **Figure 3.8b**. The ICP measurements were also conducted towards cycled electrolytes and cycled Li anodes to further quantitative analyses on Mn/Ni ions existed in cycled cells. Specifically, as shown in **Figure 3.9c**, great amount of adverse Mn/Ni dissolution can be founded within the Celgard separator based LNMO cell, while on the contrary, the cell assembled with MOF demonstrated only trace amount of Mn/Ni dissolution (Mn and Ni both increased from 0.8 k ppm at 50th cycle to nearly 4.0 k ppm at 200th cycle and stabilized at 4.1 k ppm after 500 cycles). This is in sharp contrast to that of the LNMO cell that assembled with Celgard separator (Mn sharply rises up from 30 k ppm to 48 k ppm, Ni changes from 25 k ppm to 38 k ppm, from 50th cycle to merely 200th cycle). The apparently eliminated Mn/Ni dissolution can be ascribed to the use of MOF based in-built water scavenger, which can protect the cell free from detrimental HF attack induced by the existence of water.

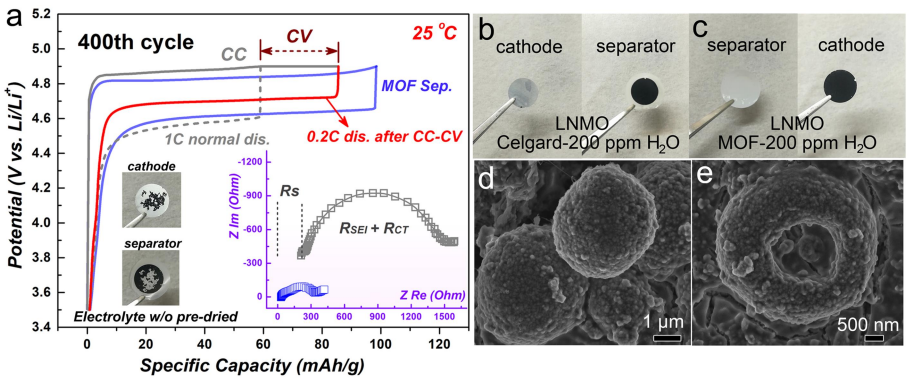

Figure 3. 10 (a) An additional electrochemical treatment on the cycled Li//LNMO cells (MOF separator based cell, the blue trace; Celgard separator based cell, the light grey and red traces). (b-d) Digital photos and SEM image of the cycled LNMO cathodes from the Celgard and MOF separators based cell (deliberately cycled in 200 ppm water added electrolyte).

In fact, both the Mn/Ni dissolved in electrolytes and re-deposited on the surface of cycled Li anodes was originally come from the LNMO cathodes. Hence, besides the Li anode degradations partially caused by Ni/Mn corrosion, the Ni/Mn loss from the LNMO cathodes can also lead to capacity decay of the LNMO cells, which was verified by the by the capacity gap between the MOF in-built water scavenger used LNMO cell and the Celgard used LNMO cell with refresh Li anode (**Figure 3.8b**, more than 20 mAh g^{-1}). In addition, we also found the serious peel off phenomenon founded in the Celgard separator used LNMO cell (**Figure 3.10b**) was significantly suppressed in MOF based in-built water scavenger used cell (**Figure 3.10c**). The corresponding EIS results also suggested that much larger resistance can be detected for cell using Celgard separator, which was caused by the poor electrical contact problem caused by the delamination of the LNMO. The CC-CV curves further verified that the increased resistance also contributed to the capacity decay of the Celgard separator based LNMO cell (**Figure 3.10a**). Since the cycled LNMO particles from the MOF used cell exhibits well-preserved spherical morphology

(**Figure 3.10d** and **e**), we think MOF based in-built water scavenger can protect the LNMO cathode materials against notorious transition metal dissolution which induced by water existed in cells.

Based on those obtained results, the capacity decay observed inn LNMO cell using Celgard separators can be ascribed to the (1) serious Mn/Ni dissolution, (2) the following increased resistance issue caused by Mn/Ni dissolution and (3) the degradation problem of Li anode. All the three issues were closely related to HF/H^+ attacks induced by reaction between H_2O and $LiPF_6$ in LIBs/LMBs as schematically illustrated in **Figure 3.1**. The enhanced electrochemical performance combined with afore-discussed measurements together verify the significant role of CuBTC MOF based in-built water scavenger in protecting the LNMO cell free from various water induced detrimental issues.

3.5 Cycling performance of lithium-metal batteries with MOF as in-built water scavenger under harsh environment (200 ppm water, 55 °C)

Inspired by those encouraging results, we begun to think about the possibility of using MOF based in-built water scavengers for LMBs under harsh environment (200 to 500 ppm water contained electrolytes, elevated temperature: 55 ^oC). Aiming to explore this possibility, various electrolytes with different amount of water additions were firstly prepared (from 200 ppm to 500 and 800 ppm) for LMBs electrochemical tests.

Electrolyte containing 200 ppm water (shorted as E-200) was initially used for various LMBs. Celgard separator and MOF based in-built water scavenger was firstly assembled and tested in Li//Li symmetrical cells. As can be found clearly, when cycled within E-200, the Li//Li cell assembled with Celgard exhibits a rapidly voltage

diverge to beyond 300 mV only after 180 hours and experienced severer sporadic voltage spikes among the whole cycling process (**Figure 3.11a**, grey trace). For sharp contrast, the MOF based Li//Li cell, surprisingly, demonstrated ultra-stable cycling performance for 2000 hours life companied with small voltage profiles (**Figure 3.11a**, blue trace). The largely improved Li//Li symmetrical performance suggests the enhanced reversibility of Li stripping/platting procedure, which was benefited from the greatly suppressed water induced HF corrosion by using MOF based in-built water scavenger. The enhanced Li//Li reversibility also consisted with the result obtained in **Figure 3.8b** and holds promising prospect for the development of long life-span LMBs.

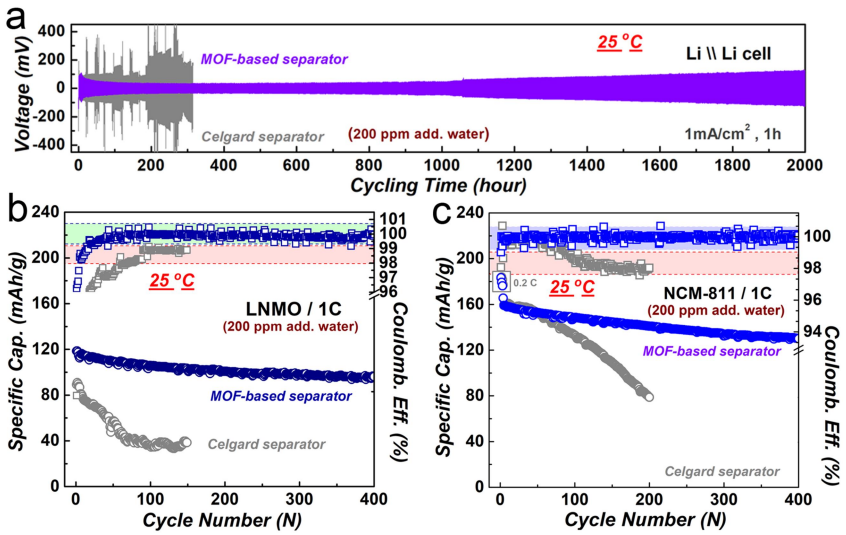

Figure 3. 11 (a) Li//Li symmetrical cell electrochemical performances of Celgard separator and MOF based in-built water scavenger cycled in electrolyte contain 200 ppm water (at a current density of 1 mA cm^{-2}). Cycling performances of Celgard separator and MOF based in-built water scavenger based (b) Li//$LiNi_{0.5}Mn_{1.5}O_4$ cells and Li//$LiNi_{0.8}Co_{0.1}Mn_{0.1}O_2$ cells at 25 °C under 1 C current rate (defined 1 C = 200 mA g^{-1}).

High-voltage cathode materials like $LiNi_{0.5}Mn_{1.5}O_4$ (LNMO) and $LiNi_{0.8}Co_{0.1}Mn_{0.1}O_2$ (NCM-811) were also tested in E-200 with both Celgard

separator and MOF based in-built water scavenger. When cycled under room temperature (25 °C) in E-200 at current rate of 1 C (1 C = 200 mA g^{-1}), the $LiNi_{0.5}Mn_{1.5}O_4$//Li (shorted as LNMO) cell assembled with MOF in-built water scavenger demonstrated long cycling life of 400 cycles and preserved above 80 % capacity (95 mAh g^{-1}) as shown in **Figure 3.11b** (blue curve). As sharp contrast, the LNMO cell assembled with Celgard separator however, experienced faster capacity decay from 84 mAh g^{-1} to only 40 mAh g^{-1} after 150 cycles (**Figure 3.11b**, grey curve). The $LiNi_{0.8}Co_{0.1}Mn_{0.1}O_2$//Li (shorted as NCM-811) also exhibit the similar results (MOF based: started at 167.5 mAh g^{-1} and sustained at 131.5 mAh g^{-1} after 400 cycles; Celgard based: with only 40 mAh g^{-1} preserved after merely 150 cycles) as that obtained in LNMO cells (**Figure 3.11c**).

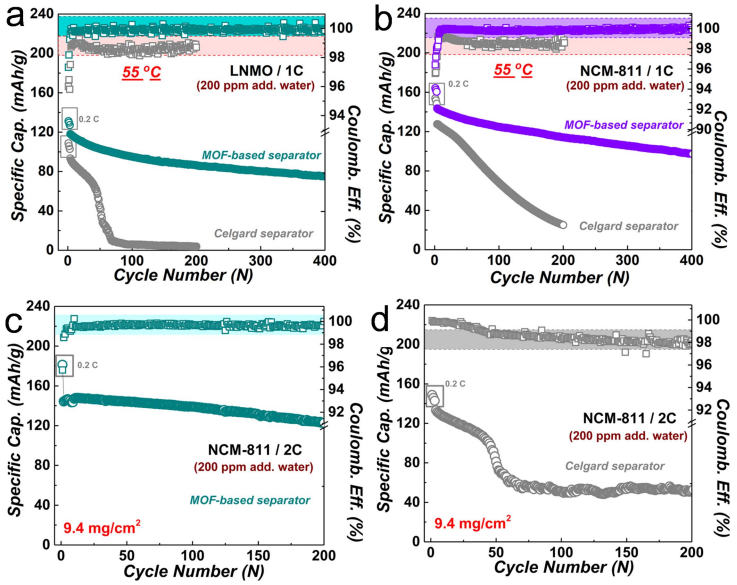

Figure 3. 12 Cycling performances of Celgard separator and MOF based in-built water scavenger based (a) Li//LiNi0.5Mn1.5O4 and (b) Li//$LiNi_{0.8}Co_{0.1}Mn_{0.1}O_2$ cells at 55 °C. (c) Cycling performances of the Li//$LiNi_{0.5}Mn_{1.5}O_4$ and (d) Li//$LiNi_{0.8}Co_{0.1}Mn_{0.1}O_2$ cells at 25 °C under high cathode mass loading of 9.4 mg/cm2.

Moreover, the high temperature performances of the two high-voltage cathodes

were also evaluated since it is widely acknowledged that server transition metal dissolutions caused by HF can be found at evaluated temperature.[37, 38] As shown in **Figure 3.12a** and **b**, even tested in harsh environment of E-200 and high temperature of 55 °C, the MOF based in-built water scavengers used LNMO and NCM-811 cells inspiringly delivered significantly enhanced performances compared with Celgard separators assembled cells.

In addition, the NCM-811 cells under high cathode loading (9.4 mg/cm^2) were also tested within E-200 electrolyte. As can be observed clearly in **Figure 3.12c**, after MOF film was used as in-built water scavenger, the NCM-811 cell can still delivered enhanced cycling performance (maintained at 120 mAh g^{-1} after cycled for 200 cycles at 2 C) compared with that using Celgard separator (**Figure 3.12d**, dropped from 147 to merely 55 mAh g^{-1} after 63 cycles).

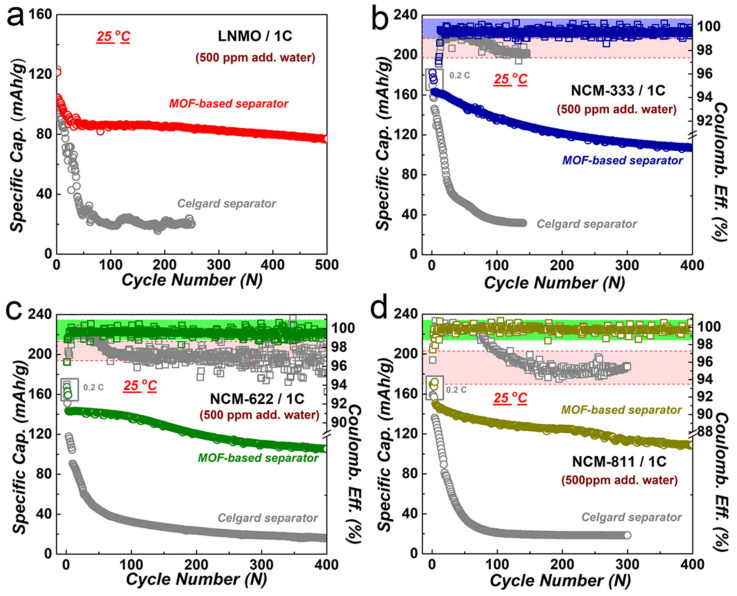

Figure 3. 13 Cycling performances of (a) Li//$LiNi_{0.5}Mn_{1.5}O_4$ (LNMO), (b) Li//$LiNi_{0.3}Co_{0.3}Mn_{0.3}O_2$ (NCM-333), (c) Li//$LiNi_{0.6}Co_{0.2}Mn_{0.2}O_2$ (NCM-622) and (d) Li//$LiNi_{0.8}Co_{0.1}Mn_{0.1}O_2$ (NCM-811) cells with Celgard and MOF based separators at 1 C current rate cycled in electrolytes containing 500 ppm water.

When the water content was increased into 500 ppm (E-500), the MOF based

in-built water scavenger used cells (LCMO, NCM-811, $LiNi_{0.3}Co_{0.3}Mn_{0.3}O_2$ (NCM-333) and $LiNi_{0.6}Co_{0.2}Mn_{0.2}O_2$ (NCM-622)) can also delivered apparent much better cycling performances than their Celgard used counter-part (as shown in **Figure 3.13**). Considering the high water content, these results are quite inspiring. As LMBs can be normally cycled in electrolyte containing such a high amount of water, those obtained results imply that may be the complex purification processed of electrolytes can be largely simplified. As a result, the corresponding costs and energy usages are expected to be largely decreased.

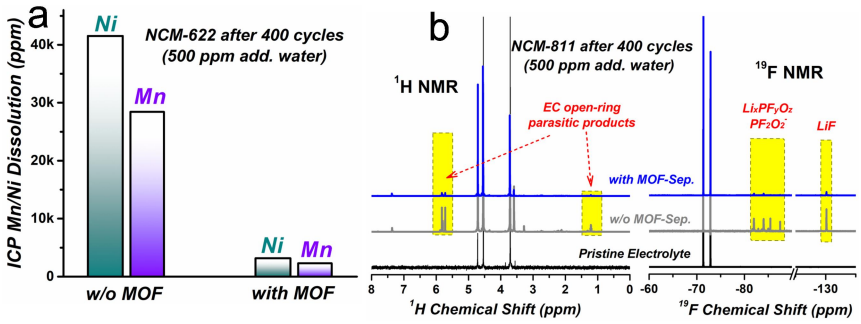

Figure 3. 14 (a) ICP analysis (Ni, Mn) results of the two Li//NCM-622 cells assembled with Celgard and MOF separators cycled in electrolytes containing 500 ppm water after 400 cycles. (b) ^{1}H NMR and ^{19}F NMR analysis results of electrolytes from two Li//NCM-811 cells assembled with Celgard and MOF separators after cycled in electrolytes containing 500 ppm water for 400 cycles.

Further ICP and NMR measurements were also tested to verify the important role of MOF based in-built water scavenger in suppressing water induced detrimental parasitic reactions. Similar as the results shown in **Figure 3.9**, MOF based in-built water scavengers used cells demonstrated remarkably suppressed Ni/Mn dissolution, EC open-ring parasitic products and accumulation of LiF, which again highlighted the important role of MOF based in-built water scavenger.

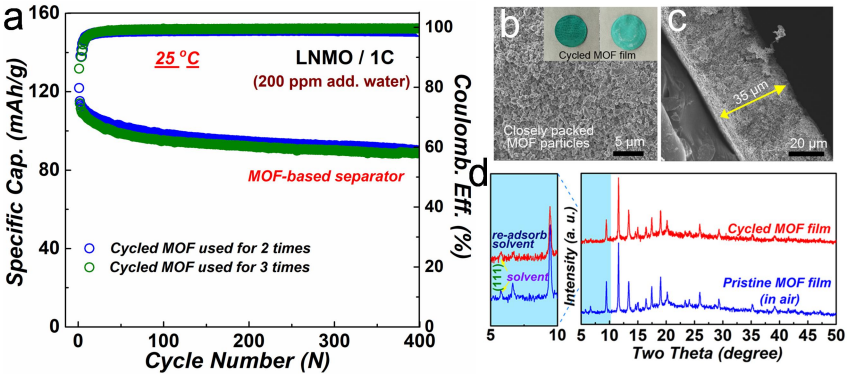

Figure 3. 15 (a) Cycling performance of the Li//LNMO cells using cycled MOF separators (blue curve for the second-hand MOF separator, green curve for the third-hand MOF separator) at 1 C current rate cycled in electrolyte containing 200 ppm water under room temperature of 25 °C.

We also repeatedly use the cycled MOF as recyclable water scavengers. After cycling, MOF based water scavenger have already adsorbed large amount of water inside their channels, which means a further re-process (re-activated procedure) are necessary before being re-used. Therefore, second hand and third hand MOF films (harvested from cycled LNMO cells) were re-assembled into LNMO//Li cells. As shown in **Figure 3.15a**, both of the two cells demonstrated excellent electrochemical performances similar as that used new MOF based in-built water scavengers demonstrated in **Figure 3.11**. In addition, the cycled MOF film was quite stable even after 2-3 rounds cycling (**Figure 3.15b-d**).

3.6 Summary and conclusions

Here, in this study, exempting from cumbersome and time/energy-consuming industrial water-removal procedures, we firstly provide an effective way to scavenge water within batteries by simply introduced metal-organic framework (MOF) into the internal of cells as efficient in-built water scavenger. Through using this simple method, water contained in cells was greatly restrained, resulting in largely suppressed electrolytes hydrolysis, HF accumulation, and transition metal dissolution

from cathodes. As a result, paring MOF separator with various high-energy-density cathodes ($LiNi_{0.5}Mn_{1.5}O_4$, $LiNi_{0.8}Co_{0.1}Mn_{0.1}O_2$ etc.), we demonstrated superior cycling stability (72% capacity retention after 400 cycles for $LiNi_{0.8}Co_{0.1}Mn_{0.1}O_2$, calculated from the 4th cycle after 3 cycles activation) even under harsh environment (200 ppm water contained electrolyte).

On mechanism level, this study originally employed MOF separator greatly suppressed transition metal dissolution of lithium-ion batteries (LIBs)/lithium-metal batteries (LMBs) by scavenging water containing in cells, resulting in remarkable enhanced LIBs performances. On practical level, introducing MOF separator into LIBs originally explores a simple but effective method in permanently restraining the detrimental influence caused by water existed (electrolyte residuals and electrolyte decomposition) in batteries. At industrial level, simply using a thin MOF separator as recyclable water scavenger can largely reduce the manufacturing costs of LIBs while improve their lifespan and safety simultaneously. Introducing small amount of MOF, one of the hot materials, enabled inspiring remarkable enhanced electrochemical performance will also provide an enlightening insight to the construction of various advanced high-energy-density electrochemical energy storage applications.

Chapter 4. An over-saturated carbonate electrolyte regulated by MOF channels eliminate electrolyte decomposition in high-energy-density lithium-metal batteries

4.1 Introduction.

Lithium-metal batteries (LMBs) have attracted lots of attention due to their potential to provide remarkably high energy density compared to conventional graphite based lithium-ion batteries (LIBs).[6, 7, 10, 18] Nevertheless, the development of LMBs has been caught in a dilemma regarding the choice of electrolyte systems, which play an essential role in enabling the battery anode and cathode (high-voltage cathodes) chemistries.[23, 44, 95, 96] Carbonate electrolytes that mainly used in graphite based LIBs for example, cannot be used in high-voltage LMBs owing to their incompatibility with Li metal anode. Highly porous and dendritic Li commonly observed in organic carbonate electrolytes, can lead to very low lithium Coulombic efficiencies (CEs) due to excessive side reactions and impose potential safety hazards due to dendrite penetrations.[45, 97, 98] Ether-based electrolytes on the other hand, though are highly compatible with metal Li, however, are excluded from being used as working electrolytes for high-voltage LMBs due to their poor oxidation stability, which are generally lower than 4.0 volts.[21, 43, 96] It is a great challenge to find electrolytes which have good compatibility with both the highly-reactive Li and the catalytic cathodes. As a result, the practical performance of high-energy-density LMBs is limited to only few cycles with low energy efficiency, remaining the development of practical long life-span high-energy-density LMBs deeply sinks into dilemma.[21, 43, 96]

Totally different from typical liquid highly-concentrated electrolyte, we

originally discovered a unique over-saturated carbonate electrolyte to overcome the aforementioned inherent drawbacks of conventional carbonate/ether electrolytes. This new electrolyte possessed a over-saturated concentration, which cannot be obtained by typical dissolution system/procedure. Benefitting from the channel within MOF-based framework, we pre-loaded trace amount of carbonate electrolyte into the MOF-model, resulting in a "over-saturated" electrolyte environment. This new electrolyte configuration renders the over-saturated carbonate electrolyte was even much stable than any commonly used highly concentrated electrolytes, and make it compatible with both oxidative high-voltage cathodes and reductive Li-metal anodes (enlarged the stability window from 4.5 V to 5.4 V, and much stable lithium reversibility). More importantly, benefited from the same reason, the solvent-depleted carbonate electrolyte composed of only tiny liquid solvents, which are favorable for the construction of high-energy-density LMBs. As a result, after matched with high-voltage cathodes ($LiNi_{0.8}Co_{0.1}Mn_{0.1}O_2$ and 5.3 V-class $LiCoMnO_4$, >9.2 mg cm^{-2}) and limited Li-metal (one time excess Li), the LMB full-cells presented life-span of 160 cycles and delivered high output energy density (630 and 670 Wh kg^{-1} ($g_{cathode+anode}$), respectively). This is a very intriguing result and far surpass the practical state-of-art LIBs. Even under harsh practical condition (ultrathin Li of 37 μm, cathode mass loading above 18 mg cm^{-2}). We anticipate that the finding will remedy the inherent defects of conventional liquid electrolytes and push the development of high-energy-density LMBs into practical commercial applications.

4.2 Inherent drawbacks of conventional liquid electrolytes

As discussed in the introduction part in **4.1**, in order to achieve high-energy-density of LMBs, highly-efficient electrolytes which are compatible to both high-voltage cathode materials and metallic Li anodes are extremely desired.[43, 96]

However, as it is widely acknowledged that neither ether-based electrolytes nor carbonate-based electrolytes are actually, not perfect. For example, for ether-based electrolytes, since are highly compatible with lithium-metal anodes, however, cannot withstand high-voltage cathode materials due to their poor oxidative stability (**Figure 4.1**, usually lower than 4.0 V). As for carbonate electrolytes, on the contrary, while can be cycled normally with high-voltage cathode materials (generally higher than 4.0 V), however, are not friendly towards lithium-metal anodes (**Figure 4.1**, right).[43, 96] As a result, it is of great significance to find or prepare other functional electrolytes which are necessary for the achieving of high-energy-density LMBs.

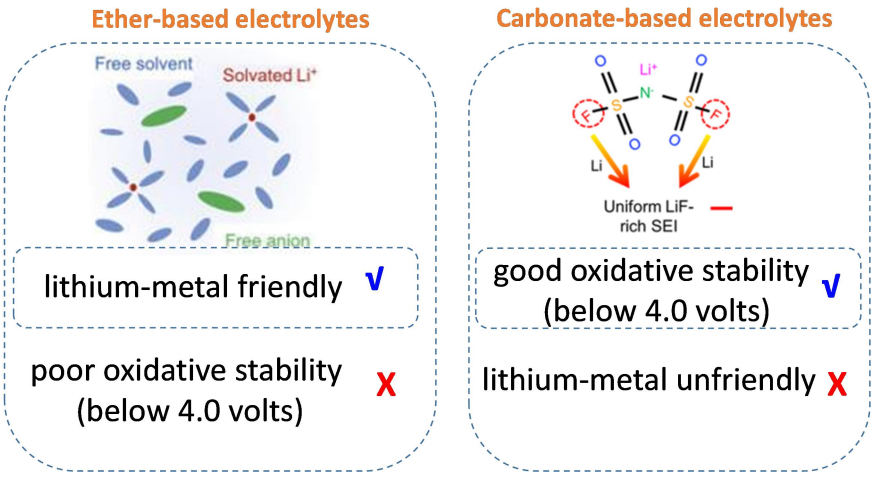

Figure 4. 1 Inherent defects of the existed liquid electrolytes in LIBs/LMBs.

During the past few years, various electrolytes have been designed for high-voltage LMB/LIBs. Among them, concentrated electrolytes have attracted most of the interests from scientific researchers around the world.[22, 23, 99-103] For example, Wang and co-authors had reported breaking finding about using highly concentrated electrolytes for LIBs.[22, 47, 101] Watanabe group,[104] Zhang group[43, 45] and Yamada group[23] also devoted their research attentions in this field. By increasing the dosage of lithium salts, electrolytes with enhanced concentrations can be obtained. Owing to the increased salt concentrations, the configurations of electrolytes were dramatically changed compared with that of the diluted electrolytes that without adding extra

amount of lithium salts. Benefit from the special configurations, concentrated electrolytes possess multiple inspiring advantages as shown in **Figure 4.2**. Despite those mentioned unique physicochemical properties demonstrated, concentrated electrolytes do have several inherent drawbacks that hindered their further applications in LMBs/LIBs. For example, the increased viscosities, largely decreased lithium-ion conductivities may lead to depressed electrochemical performances and even cause safety hazards due to the heat accumulated by lithium-ion transporting in viscous electrolytes.[23] Though local concentrated electrolytes were also further designed, the climb in the overall costs due to the additional added solvents involved however, greatly hinder their applications.[52, 99] More importantly, even enhanced electrochemical performances were obtained by using those functional concentrated/local concentrated electrolytes, the serious decomposition of electrolyte components, however, still exist and damage both the cathodes and anodes.[23, 44] To eliminate/suppress the disadvantages of those existed electrolytes, electrolytes with novel configurations need to be designed.

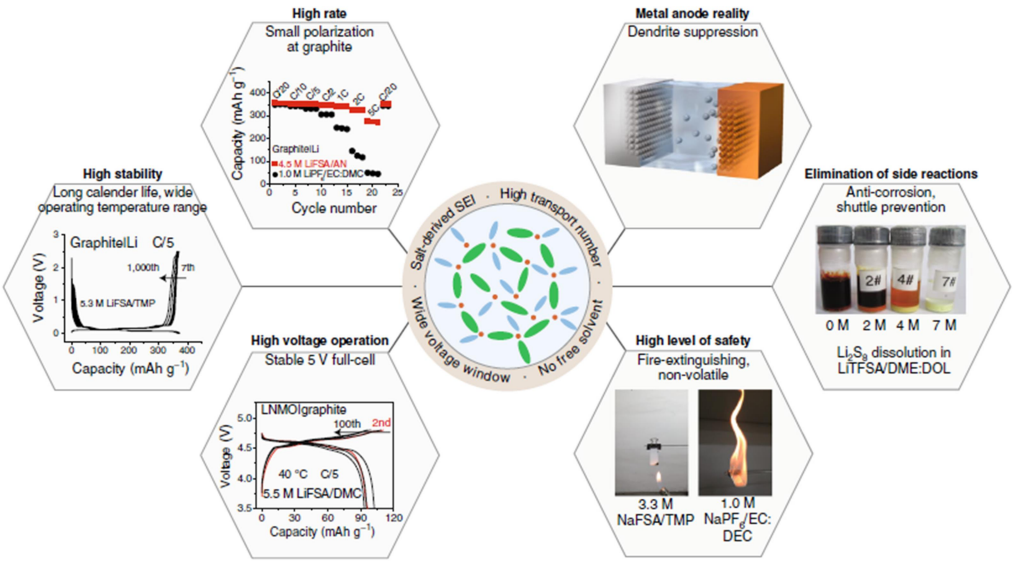

Figure 4. 2 Schematic illustrations of various advantages for concentrated electrolytes.[23] Reproduced with permission from ref. 23. Copyright 2019, Nature

Publishing Group.

4.3 Unique electrolyte configuration regulated inside MOF channels

It is widely acknowledged that the configurations of electrolytes greatly influence their physicochemical properties, which consequently affect the electrochemical performances of LMBs/LIBs after assembled with those electrolytes.[23, 44] Thus, our primary target is to design electrolyte with unique configuration, which is even more aggregated than concentrated electrolytes.

Owing to their unique nano/sub-nano structures, metal-organic frameworks (MOFs) have received numerous research attentions in LMBs/LIBs. Several works have reported enhanced electrochemical stabilities after MOFs were employed to regulate the properties of conventional electrolytes.[70] Among them, Lu group[66, 90] and Pan et al.[48, 86] are one of the pioneers. Conceptually different from those works (in which MOFs were simply mixed with electrode materials, binders and conductive carbons), we would like to encapsulate liquid electrolyte inside MOF channels. After the liquid electrolyte was filled inside MOF channels, we begun to unveil the physicochemical properties of the MOF regulated electrolyte. Propylene Carbonate/LiTFSI (PC/LiTFSI) based carbonate electrolyte was used as both the precursor electrolyte and comparative electrolyte sample. Space-resolution operando Raman and Fourier-transform infrared spectroscopy (FT-IR) technologies were firstly adopted to characterize the configuration of electrolyte confined inside MOF channels in detail. Both PC and PC-LiTFSI electrolyte were recorded as calibrators. As shown in **Figure 4.3**, for PC solvent, Raman shift demonstrates apparent -O-C(=O)-O- asymmetric stretching (from PC, at 711.7 and 1229.8 cm^{-1}).[105] IR spectrum shows clearly the existence of out-of-plane ring deformation (776.8 cm^{-1}) peak of PC. In addition, other two peaks situated at 1350 cm^{-1} and 1391.7 cm^{-1} can be ascribed to

the C-H bending and $–OCH_2$ wagging of PC, respectively.[106] Peaks related to Li^+-PC interactions can also be clearly detected in both Raman (1245.9 cm^{-1}) and IR (727.5 and 1405.1 cm^{-1}) after 1M LiTFSI salt was added.[107] We can also found a newly appeared peak in Raman spectrum situated between 740-744 cm^{-1}, which can be assigned to the SNS stretching of $TSFI^-$.[108] This new peak can be split into two individual peaks which present the "SSIP (solvent separated ion pair)" and "CIP (contact ion pair)" modes between Li^+ and $TFSI^-$. After saturated PC-LiTFSI electrolyte was under evaluation, remarkable change can be observed between 740-744 cm^{-1} in Raman spectrum: in where the SNS stretching of $TSFI^-$ evolved from "SSIP" dominated to "CIP" dominated. In addition, enhanced peak intensities related to Li^+-PC interactions in IR can also be observed. Interestingly, when MOF filled with electrolyte was employed, significant changes can be clearly found. Specifically, Raman shift situated between 700-800 cm^{-1} exhibits the most apparent change: the peak related to the SNS stretching of $TFSI^-$ composed of only CIP mode. Moreover, the peak intensity that originally related to skeletal bending (711.6 cm^{-1}) transformed into a relatively weak but broad peak, in which an enhanced peak of Li^+-PC interaction (**Figure 4.3**, top) can be obtained. The corresponding IR spectra also exhibited largely enhanced peak intensities reflected Li^+-PC interaction compared with that of saturated carbonate electrolyte. Since there was still SSIP mode of $TFSI^-$ can be found in saturated electrolyte, it is hence reasonable to conclude that electrolyte confined inside MOF channels possessed a higher concentration than saturated electrolyte, therefore, we defined this electrolyte inside MOF channels as over-saturated electrolyte.

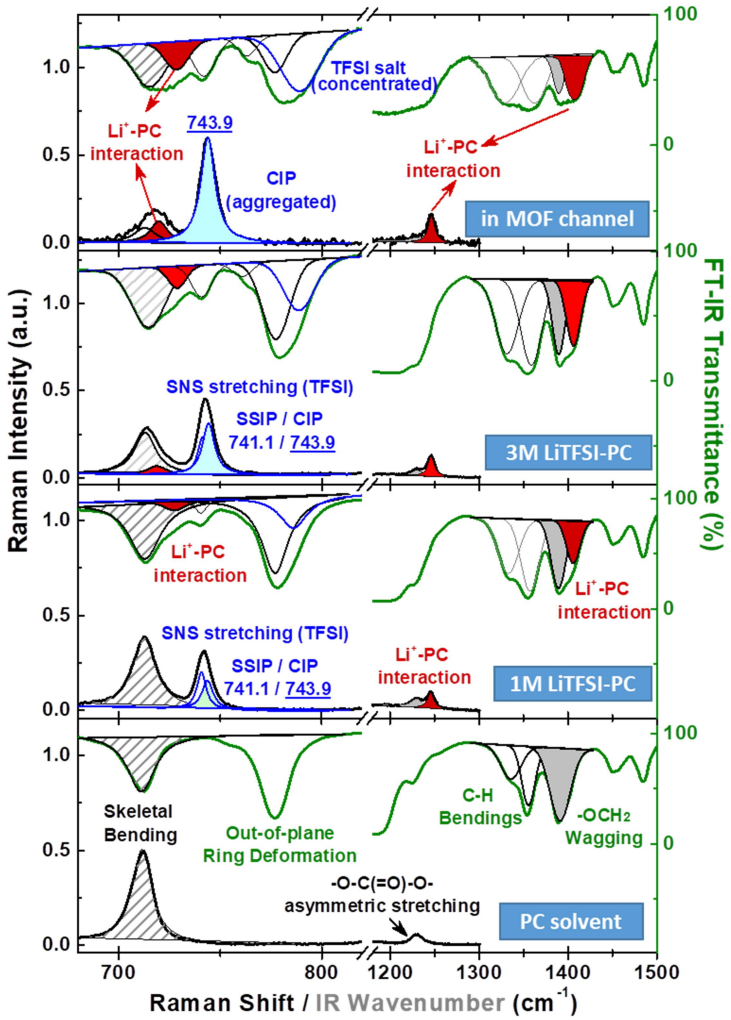

Figure 4. 3 Raman and FT-IR spectrum of the prepared over-saturated carbonate electrolyte.

4.4 Electrochemical properties of the over-saturated carbonate electrolyte realized inside MOF channels

As the special over-saturated electrolyte was obtained, the corresponding electrochemical properties were also under further evaluations. Firstly, linear sweep voltammetry (LSV) of both the PC-LiTFSI electrolyte and the MOF regulated oversaturated electrolyte test were tested. Clearly, for the 1M PC-LiTFSI electrolyte (**Figure 4.4a**, grey curve), the corresponding LSV curve suggested the mediocre oxidation stability (around 4.5 V, compatible with high-voltage cathode materials),

which is consist with general knowledge. Inspiringly, for the obtained over-saturate electrolyte, largely expended electrochemical voltage window of 5.4 V can be observed (**Figure 4.4a**, blue curve). We ascribe the largely improved oxidation stability of the over-saturated electrolyte to the special electrolyte configuration achieved inside the narrow channels of MOF.

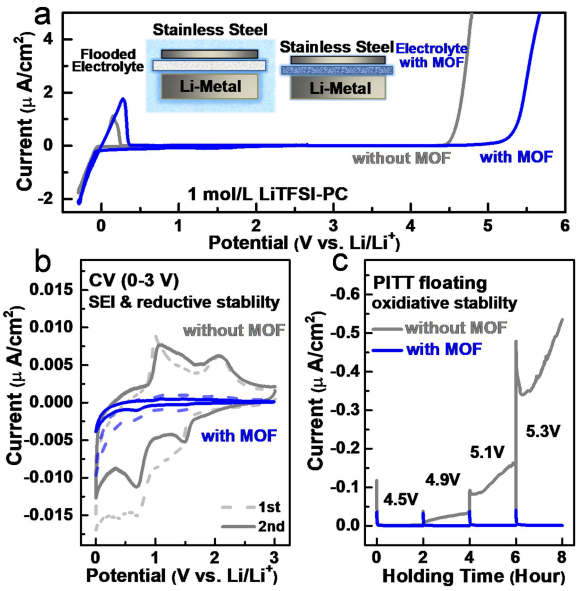

Figure 4. 4 (a) Linear sweep voltammetry (LSV) curves of the two carbonate electrolytes (blue curve: PC-LiTFSI with MOF (over-saturated carbonate electrolyte); light grey curve: PC-LiTFSI without MOF). The inset schematically illustrates the different cell configurations. (b) Cyclic voltammograms (CV) indicates the enhanced reductive stability of the over-saturated carbonate electrolyte. (c) Potentiostatic Intermittent Titration Technique (PITT) floating test suggests greatly enhanced oxidative stability of the super-solubility concentrated carbonate electrolyte.

Cyclic voltammograms (CV) curves of the two electrolytes were also tested (the initial two cycles) to study the corresponding surface layer formation behaviors (**Figure 4.4b**). As can be found clearly, the over-saturated electrolyte demonstrated both much superb solid electrolyte interface (SEI) formation and apparently stable reductive ability when compared with that of the conventional PC-LiTFSI

electrolyte.[109] In addition, the Potentiostatic Intermittent Titration Technique (PITT) floating tests were also tested. As can be found in **Figure 4.4c**, the over-saturated electrolyte demonstrated apparently remarkably enhanced oxidative stability when charged to different high-voltages (from 4.5 V to 5.3 V). For sharp contrast, the PC-LiTFSI however, experienced severer oxidative decompositions under the same environment. Until now, the prepared over-saturated electrolyte has demonstrated excellent physicochemical properties compared with the conventional PC-LiTFSI electrolyte. This indicates that the prepared over-saturated electrolyte is promising to be used as functional electrolyte for high-voltage LMBs.

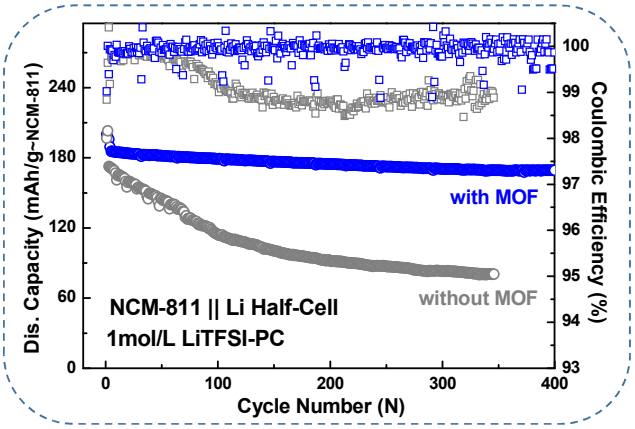

Figure 4. 5 Cycling performance of the NCM-811//Li half-cell using two different carbonate-based electrolytes (blue curve: 1 M PC-LiTFSI with MOF (over-saturated electrolyte); light grey curve: 1 M PC-LiTFSI without MOF).

To further verify the superiority of the prepared over-saturated carbonate electrolyte (1M PC-LiTFSI with MOF) on the electrochemical performances of high-energy-density LMBs, $LiNi_{0.8}Co_{0.1}Mn_{0.1}O_2$ (shorted as NCM-811) cathode coped with Li-metal anode ($LiNi_{0.8}Co_{0.1}Mn_{0.1}O_2$//Li cell, defined as NCM-811//Li,) was firstly tested as shown in **Figure 4.5**. Compared with NCM-811//Li cell assemble with conventional carbonate based 1M PC-LiTFSI electrolyte (grey curve, without MOF), the NCM-811//Li cell assembled with over-saturated carbonate electrolyte (1M PC-LiTFSI with MOF, blue curve) exhibits both much better cycling stability and

higher Coulombic efficiency (CE). Specifically, NCM-811//Li cell assemble with over-saturated carbonate electrolyte (1M PC-LiTFSI with MOF) delivered an initial capacity of 190 mAh g^{-1} (recorded at the 2nd cycle, since the first cycle was activated at 0.1 C) and maintained at 170 mAh g^{-1} after 400 cycles, corresponding to nearly 90% capacity retention and a slow capacity decay of 0.026% per cycle (unlimited Li, ~200 μm). This is in sharp contrast to that of conventional carbonate electrolyte used cell, whose capacity experienced a quick drop (dropped from 174 mAh g^{-1}) with only 81 mAh g^{-1} was preserved after merely 348 cycles (corresponding to 46% capacity retention). Moreover, the Coulombic efficiency of the over-saturated carbonate electrolyte (1M PC-LiTFSI with MOF) based NCM-811//Li cell was also higher than its counterpart. The reason for the apparently improved electrochemical performance needs further investigations.

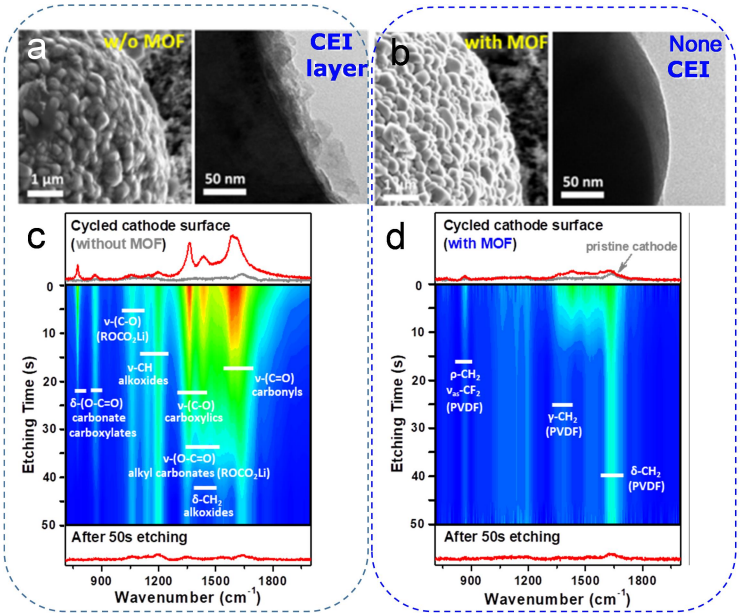

Figure 4. 6 SEM and TEM images of the cycled NCM-811 cathodes within (a) common carbonate electrolyte (1 M PC-LiTFSI without MOF) and (b) over-saturated carbonate electrolyte (1 M PC-LiTFSI with MOF). The etching FT-IR spectra of the cycled NCM-811 cathode using (a) common carbonate electrolyte and (b) over-saturated carbonate electrolyte.

Cycled NCM-811 cathodes harvested from two electrolytes were also under further Scanning Electron Microscope (SEM) and Transition Electron Microscope (TEM) investigations (as shown in **Figure 4.6a** and **b**) to further explore the reason for the apparently improved electrochemical performance by using newly designed over-saturated carbonate electrolyte (1M PC-LiTFSI with MOF). For the NCM-811 cathode within conventional carbonate electrolyte (1M PC-LiTFSI without MOF), the unevenly covered cathode electrolyte interface (CEI) layer can be clearly observed (**Figure 4.6a**). For sharp contrast, the NCM-811 cell cycled in the newly designed over-saturated carbonate electrolyte (1M PC-LiTFSI with MOF), surprisingly, do not exhibited any cathode electrolyte interface (CEI) layer (**Figure 4.6b**). This demonstrated the important role of the newly designed over-saturated carbonate electrolyte (1M PC-LiTFSI with MOF) in suppressing the long-lasting serious decomposition of electrolyte on the surface of catalytic NCM-811 cathodes.

Etching FT-IR experiment was also employed to exam the surface properties of the cycled NCM-811 cathodes as shown in **Figure 4.6c** and **d**. Apparently, for NCM-811 cathode assembled with conventional carbonate electrolyte, we can found obvious peaks which can be assigned to the side-reaction parasitic products caused by electrolyte solvent related decomposition during the long etching time and depth. Strong peaks located at 1355, 1436 and 1596 cm^{-1} are related to carboxylics (C-O), alkyl carbonates ($ROCO_2Li$) and carbonyls (C=O), respectively.[96] These peaks closely related to the decomposition of electrolyte solvents. As a comparison, only tiny PVDF related peaks can be observed in over-saturated electrolyte used NCM-811 cathode, which indicated almost totally eliminated electrolyte decomposition as shown in **Figure 4.6d**.

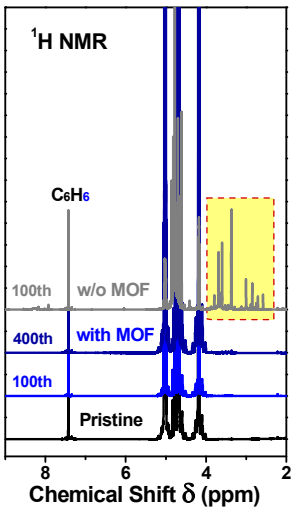

Figure 4. 7 ^{1}H NMR analysis results of cycled electrolytes showing greatly restrained decomposition of electrolyte in NCM-811//Li cell using over-saturated carbonate electrolyte (1 M PC-LiTFSI with MOF).

Electrolytes collected from the two cycled cells were also submitted to Nuclear Magnetic Resonance (NMR) measurement (^{1}H of D_2O) to characterize further information. As can be found in **Figure 4.7**, compared with the electrolyte that harvested from conventional carbonate electrolyte used NCM-811//Li cell (grey curve, yellow highlighted), electrolyte harvested from over-saturated electrolyte used cell demonstrated significantly suppressed electrolyte open-ring parasitic products (blue curves after 100 and 400 cycles). It is hence reasonable to conclude that PC solvents decomposition in over-saturated electrolyte used cell was remarkably eliminated, which directly demonstrated the advantage of the unique electrolyte configuration.

4.5 Improved compatibility of the over-saturated carbonate electrolyte toward lithium-metals

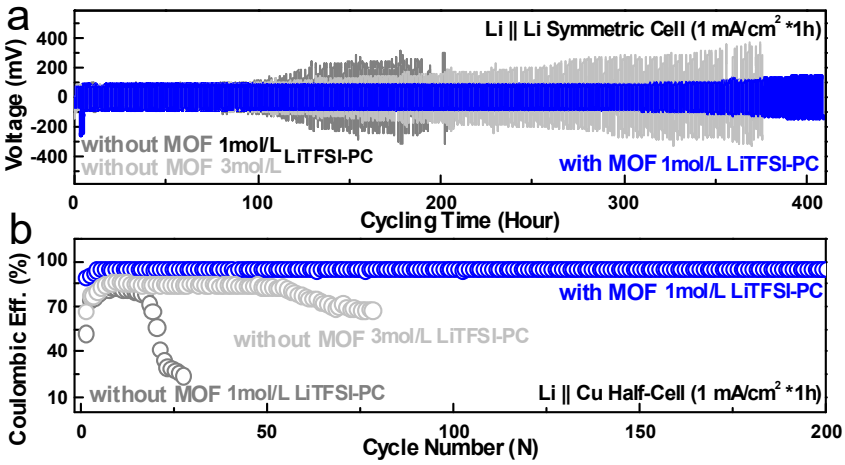

Figure 4. 8 (a) Li//Li symmetrical cells performances cycled within two different carbonate based electrolytes (blue curve: PC-LiTFSI with MOF; light grey curve: PC-LiTFSI without MOF) at current density of 1 mA cm^{-2}. (b) Coulombic efficiency (CE) of the Li//Cu half-cells using common carbonate electrolyte and the over-saturated carbonate electrolyte at current density of 1 mA cm^{-2}.

Those obtained inspiring results show promising prospect of using the over-saturated electrolyte to construct high-voltage lithium-metal full-cells. Before the fabrication of high-voltage lithium-metal full-cells, the Li plating/stripping reversibility of two electrolytes were firstly evaluated in Li//Li symmetrical cells. When cycled in conventional carbonate electrolyte, the Li//Li cell delivered a quickly voltage deviate after merely 80 hours and exhibited serious voltage polarization beyond 300 mV after 180 hours (**Figure 4.8a**, grey trace). While for sharp contrast, Li//Li cell assembled with the over-saturated carbonate electrolyte, delivered a much better voltage profiles and longer cycling life without apparent voltage diverge (**Figure 4.8a**, blue trace, 100 mV maintained after more than 400 hours). What interested us is that the Li//Li cell performance of the over-saturated electrolyte cell

was even much better than that of the Li//Li cell assembled with saturated carbonate electrolyte (**Figure 4.8a**, dark grey trace, in which constant voltage polarization can be observed during the whole cycling process). This suggested greatly enhanced reversibility of the Li plating/stripping due to the employed of over-saturated electrolyte.

Li//Cu cells were also tested to further evaluate the performances of the prepared over-saturated electrolyte. Firstly, Li//Cu with infinite Li-metal were tested under 1 mA/cm^2 as shown in **Figure 4.8b**. We can found clearly that the over-saturated electrolyte assembled Li//Cu cell also demonstrated apparently much higher coulombic efficiency (over-saturated electrolyte: above 95%, blue curves) as well as much stable stability than that of Li//Cu cell used conventional carbonate electrolyte (dropped from 81% to 26% after only 25 cycles in diluted 1M carbonate electrolyte; dropped from 86% to 66% after 74 cycles in saturated carbonate electrolyte).

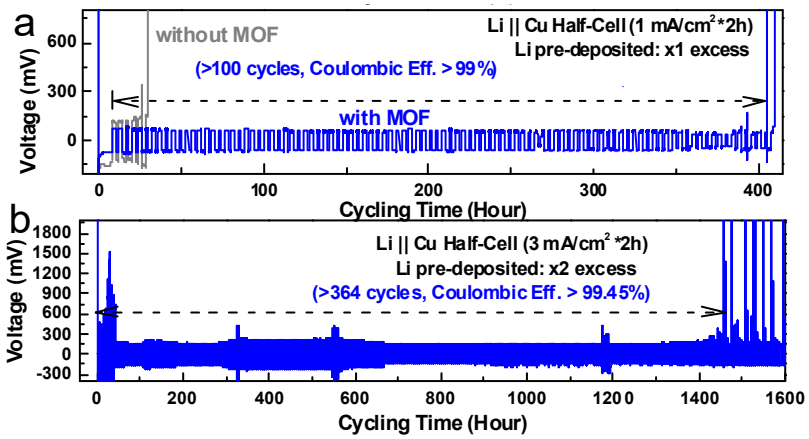

Figure 4. 9 (a) Discharge curves of the Li//Cu half-cell with once excess Li at a current density of 1 mA cm^{-2} and (b) discharge curves of the Li//Cu half-cell with two times excess Li at a current density of 3 mA cm^{-2} indicate the superb Li//Cu performance by using the over-saturated carbonate electrolyte.

Li//Cu cells with limited Li were also tested within two electrolytes. As can be found in **Figure 4.9**, both the Li//Cu cells under one time excess Li and two times excess Li together delivered nearly the same results: the over-saturated electrolyte

assembled Li//Cu cells exhibited greatly improved lifespan. Specifically, the over-saturated electrolyte assembled cell delivered a long cycling time of more than 400 hours (equals to 100 cycles, **Figure 4.9a**) and 1460 hours (above 360 cycles, **Figure 4.9b**) under 1mA cm^{-2} and 3 mA cm^{-2}, respectively. The corresponding CEs of the over-saturated electrolyte used cells were also calculated as high as 99.0%, 99.45%, respectively. The commercial carbonate electrolyte on the contrary, however, enabled much inferior Li//Cu performance with only 30 hours cycle time and extremely poor CE can be obtained (**Figure 4.9a**, grey curve).

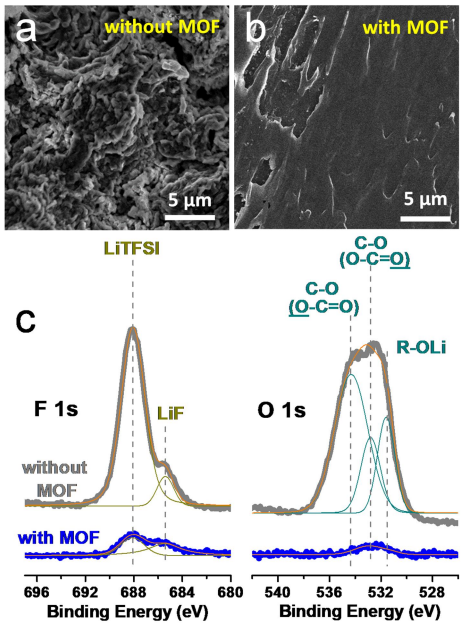

Figure 4. 10 SEM images of the cycled Li electrodes using common (a) carbonate electrolyte (after 30 hours) and (b) the over-saturated carbonate electrolyte (after 400 hours). (c) The corresponding XPS results of the cycled Li electrodes (left: F 1s; right: O 1s).

The cycled Li metals were also submitted to SEM and X-ray photoelectron spectroscopy (XPS) to further investigated their surface properties. As shown in **Figure 4.10a**, the cycled Li from conventional carbonate electrolyte exhibited seriously accumulated dendrite Li, which we think may be induced by the constant decomposition of PC solvents. Interestingly, the cycled Li metal anode from

over-saturated electrolyte exhibited smooth surface even after 400 hours cycling without any apparent dendritic Li can be found. XPS of the two cycled Li anodes harvested from different electrolytes were also recorded. As shown in **Figure 4.10c** and **d**, cycled Li from conventional carbonate electrolyte demonstrated serious electrolyte decomposition related products: R-OLi (531.5 eV), C-O (O-C=O, 532.8 eV) and C-O (O-C=O, 534.4 eV),[96] while the cycled Li from over-saturated electrolyte exhibited greatly suppressed solvent decomposition as (blue trace). We think this interesting phenomenon can be ascribed to the fact that Li did not directly contact with bulk electrolyte.

4.6 Cycling Performance of high-voltage LMB using MOF regulated over-saturated carbonate electrolyte

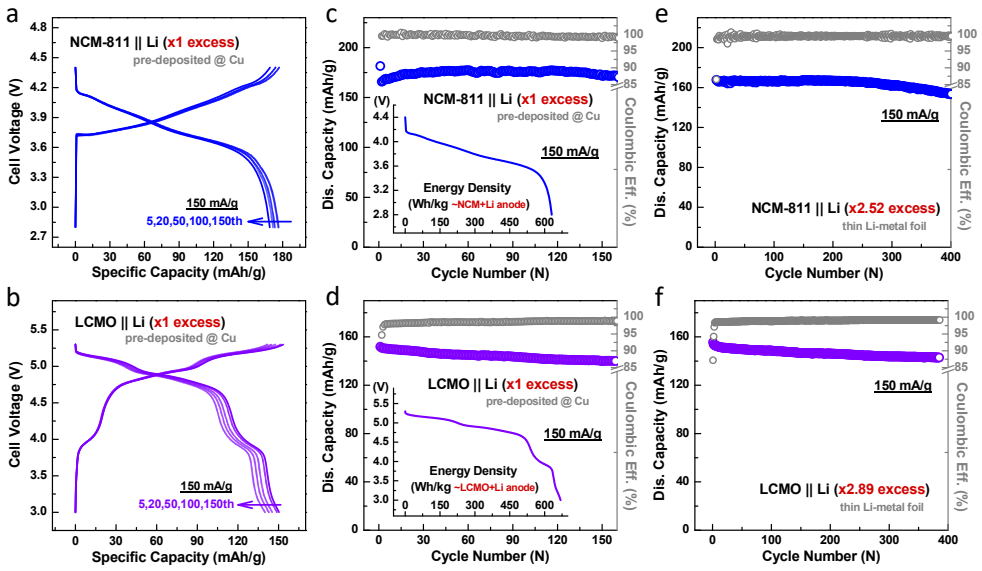

Figure 4. 11 Stable electrochemical performances of high-energy-density lithium metal batteries (LMBs) using over-saturated carbonate electrolyte under limited amounts of lithium. (a, c) Discharge capacity against cycle number and the corresponding galvanostatic discharge curves versus the gravimetric energy density (shown in the inset) of NCM-811//Li-metal full-cell (one time excess Li, current

density of 150 mAh g^{-1}) and (b, d) 5.0 V-class LCMO//Li-metal full-cell (one time excess Li, current density of 150 mAh g^{-1}) using the over-saturated carbonate electrolytes. Cycling performances of (e) NCM-811//Li full-cell under 2.52 excess Li and (f) LCMO//Li cell full-cell under 2.89 excess Li.

Those obtained excellent electrochemical and physical properties of the over-saturated electrolyte show promising prospect to build highly-efficient high-energy-density lithium-metal full-cells. So, both the NCM-811//Li and LCMO//Li cells were assembled with the over-saturated electrolyte to construct LMB full-cells and evaluate their electrochemical performances. Firstly, when one tome excess Li metal were used (calculated based on the NCM-811 cathode mass loading), as shown in **Figure 4.11 a** and **c**, the NCM-811//Li full-cell demonstrated excellent cycling performance as a high discharge capacity of 171 mAh g^{-1} after 160 cycles can be obtained. Moreover, the CE of the NCM-811//Li full-cell was calculated to be above 99.5%. In addition, we also calculated the output energy density of the NCM-811//Li full-cell. A high value of more than 630 Wh kg^{-1} (based on the total mass of NCM-811 and Li-metal) was finally achieved (as inset shown in **Figure 4.11 c**). This result is quite impressive and among the top level compared with works reported by other groups.[41, 110] LCMO//Li full-cell was also tested under one time excess Li as shown in **Figure 4.11b** and **d**. Similarly, the 5.0 V-class LCMO//Li full-cell can sustained at 140 mAh g^{-1} after 160 cycles, which corresponding to a high output energy density of more than 670 Wh kg^{-1} (as inset shown in **Figure 4.11 d**). Considering the high voltage platform of the LCMO cathode, the energy density of the LCMO//Li full-cell was even higher than that of the NCM-811//Li full-cell.

These two kinds of LMB full-cells were also further tested under a slightly higher excess Li condition. For NCM-811//Li cell which tested under 2.5 times of excessed Li, we cannot found apparent capacity decay during the whole 400 cycles

(**Figure 4.11e**, CE was recorded as high as 99.5%). For the 5.0 V-class LCMO//Li cell, despite the slight capacity decay found in the initial cycles, a high capacity of 144 mAh g^{-1} after 400 cycles can be observed as shown in **Figure 4.11f**.

These obtained results were also consisted with the CE values and cycling times of the Li//Cu cells in **Figure 4.9**. These obtained excellent electrochemical performances directly demonstrate the superiority of using the newly prepared over-saturated carbonate electrolyte for high-energy-density LMB full-cells. Considering the high cathode mass loading and thin thickness of Li metal anodes, the over-saturated electrolyte holds inspiring prospect in the construction of practical high-energy-density LMBs.

4.6 Summary and conclusions

In summary, by employing a unique over-saturated carbonate based liquid electrolyte, we demonstrated a high-energy-density rechargeable lithium-metal battery technology. Regulated by the MOF channels, the newly designed over-saturated carbonate electrolyte (Propylene Carbonate/LiTFSI (PC/LiTFSI) within MOF) composed of only tiny liquid solvents, and possessed an over-saturated concentration, which is even higher than that of any highly concentrated and saturated liquid electrolytes. More importantly, benefited from its unconventional electrolyte configuration, this special over-saturated carbonate electrolyte was verified compatible with both highly oxidative high-voltage cathodes and reductive Li-metal anodes (with remarkably enhanced lithium compatibility (greatly improved Li//Cu symmetrical cell and enhanced oxidation stability (enlarged from original 4.5 volts to 5.4 volts)). In addition, the over-saturated carbonate electrolyte was even much stable than the highly concentrated counterpart. After coped with high-voltage cathodes, ultra-stable high-energy-density lithium-metal batteries at commercial-level of areal

capacity and lifespan were also achieved (171 mAh g^{-1} maintained after 400 cycles under a high NCM-811 mass loading and ultra-thin Li (2.52 excess of Li) for NCM-811//Li cell; 144 mAh g^{-1} preserved after 400 cycles under a high LCMO mass loading and ultra-thin Li (2.89 excess of Li) for 5.0 V-level LCMO//Li cell). Meanwhile, the employment of the over-saturated carbonate electrolyte further eliminated the formation of cathode electrolyte interface (CEI) layer on the surface of high-voltage cathode caused by decomposition of electrolyte solvent molecules between the electrodes and electrolyte. We anticipate that the finding of this unique over-saturated carbonate electrolyte will remedy the inherent defects of conventional liquid electrolytes and push the development of high-energy-density LMBs to a practical commercial level.

Chapter 5. General conclusions and perspectives

5.1 General conclusions

In this dissertation, we have effectively suppressed the detrimental and long-lasting electrolyte decomposition issues existed in conventional lithium-ion batteries (LIBs) and lithium-metal batteries (LMBs) by using metal-organic frameworks (MOFs). Generally, there are two typical reasons that lead to the aforementioned electrolyte decomposition issues in LIBs and LMBs: the first one reason is the "external" factor which can be ascribed to the existence of water in electrolytes. The other one is the "internal" factor due to the inherent defects of the existed commercial electrolytes. For the first issue, we have designed one excellent MOF film based in-built water scavenger to adsorb water already contained and/or subsequently formed in LMBs cells. For the second problem, we have designed a special over-saturated electrolyte which was confined inside MOF channels to strength the stability of carbonate electrolyte. In this dissertation, through using MOFs, these two tricky issues have been greatly eliminated. All of the results were firmly evidenced by solid spectroscopies and other physical characterizations. After these notorious problems have been effectively dissolved, high-energy-density LMBs full-cells with excellent electrochemical performances were finally obtained.

In **Chapter 3**, the purpose of scavenging water in high-voltage LMBs: the "external" issue is implemented. Negative effects of water exist in lithium-metal battery and how water molecules damage the performance of high-voltage LMBs has been fully demonstrated in **Chapter 3.2.** Excellent water scavenging ability of the CuBTC MOF composites has been confirmed in **Chapter 3.3**. After been used as in-built water scavenger to extrude water existed in LMBs, excellent electrochemical performances and significantly suppressed water induced side-reactions have been

solidly confirmed in **Chapter 3.4** and **3.5**.

In **Chapter 4**, the purpose of suppressing the "internal" issue: the decomposition of electrolyte solvent molecules is achieved. Unique over-saturated electrolyte configuration regulated inside MOF channels was achieved in **Chapter 4.3**. The unique and excellent electrochemical properties (expanded voltage window, suppressed electrolyte decomposition and improved Li reversibility) of the over-saturated carbonate electrolyte realized inside MOF channels were comprehensively evaluated in **Chapter 4.4**. The prepared over-saturated electrolyte also demonstrated improved compatibility toward lithium-metals in **Chapter 4.5**. As a result, we obtained LMB full-cell with high output energy density in **Chapter 4.6**.

In general, MOFs have been introduced into the LIBs/LMBs systems aiming to dissolve several inherent long-lasting drawbacks existed in electrolytes which used in LIBs/LMBs. We need to stabilize cells and expect improved electrochemical performances by using MOFs as functional materials. The water scavenging property of the CuBTC MOF helps to extrude water existed in LIBs/LMBs, which free the cells from annoying water-related HF attack. We also go step further by confining electrolyte inside MOF channels and prepared a configuration unique over-saturated electrolyte, which exhibited excellent physicochemical/electrochemical properties. Benefit from the special electrolyte configuration, remarkably suppressed electrolyte decomposition and significantly improved electrochemical performances were finally achieved. In this dissertation, only two MOF with different properties were used. And in this research, we merely provide one access to improve the electrochemical performance of Li-metal batteries. Our works just throw a brick to the field of LIBs/LMBs and humbly hope the results will contribute to the development of Li-ion battery/Li-metal battery technology for towards high power density, long cycling life and low cost for large scale storage systems.

5.2 Perspectives

Even enhanced electrochemical performances have been achieved by using MOFs in lithium-metal batteries, however, the improvement were only obtained in only two types of electrolyte. Although we found that the configuration of electrolyte will be fundamentally changed when confined inside the channel of MOFs, we do not have enough evidences that this finding can be expanded to other electrolyte systems at this stage. Therefore, to further develop our research, other kind of electrolytes especially the ether based electrolyte and aqueous electrolytes need to be further investigated as shown in **Figure 5.1**. By confining MOF channels with different kinds of electrolytes and lithium salts, we can investigate the electrolytes' configurations in a much comprehensive way. After several electrolytes were studied, the principle law for reason of the electrolytes' configuration changes would be carried out. We think this possesses a great scope to develop highly efficient electrolytes to power high-energy-density battery technologies, which would reach far beyond Li-ion battery, Li-metal battery, etc.

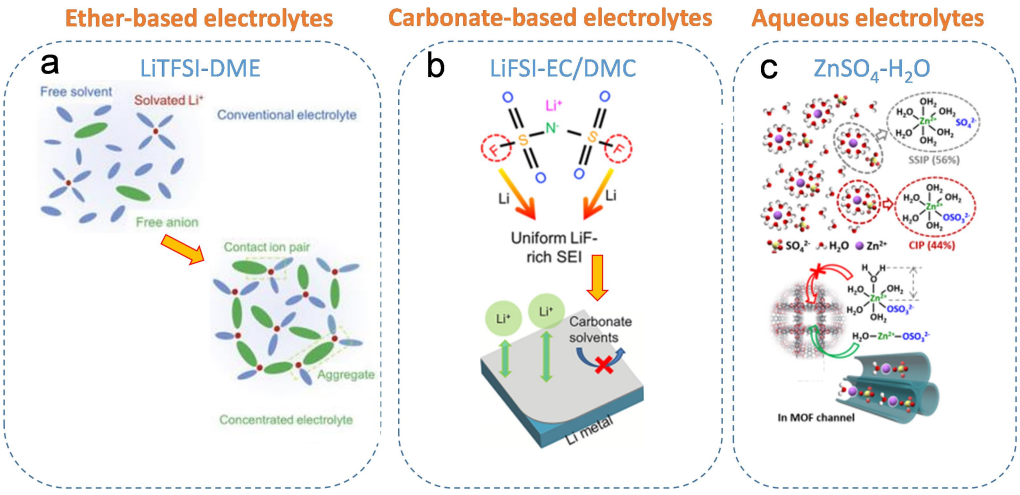

Figure 5. 1 Further study the configurations and properties of other electrolyte systems regulated inside MOF channels.[23, 101, 111] Reproduced with permission from ref. 23. Copyright 2019, Nature Publishing Group. Reproduced with permission from

ref. 101. Copyright 2018, Elsevier Inc. Reproduced with permission from ref. 111. Copyright 2020, Wiley-VCH.

List of Publications

First author:

1. **Zhi Chang**, Yu Qiao, Han Deng, Huijun Yang, Ping He and Haoshen Zhou. A stable high-voltage lithium-ion battery realized by an in-built water scavenger. *Energy & Environmental Science*, 2020, 13, 1197-1204.

2. **Zhi Chang**, Yu Qiao, Huijun Yang, Han Deng, Ping He and Haoshen Zhou. Stable high-energy-density lithium-metal batteries realized by over-saturated carbonate electrolyte system. **Submitted** to *Energy & Environmental Science.*

(**The first two papers are related to this Ph.D. thesis.**)

3. **Zhi Chang**, Yu Qiao, Han Deng, Huijun Yang, Ping He and Haoshen Zhou. A liquid electrolyte with de-solvated lithium-ions for lithium-metal battery. *Joule*, 2020, 10.1016/j.joule.2020.06.011.

4. **Zhi Chang**, Yibo He, Han Deng, Xiang Li, Shichao Wu, Yu Qiao, Pengfei Wang, Haoshen Zhou. A Multifunctional Silly-Putty Nanocomposite Spontaneously Repairs Cathode Composite for Advanced Li-S Batteries. *Advanced Functional Materials*, 2018, 28 (50), 1804777.

5. **Zhi Chang**, Yu Qiao, Jie Wang, Han Deng, Ping He, Haoshen Zhou. Fabricating better Metal-Organic Frameworks separators for Li-S batteries: pore sizes effects inspired channel modification strategy. *Energy Storage Materials* 2020, 25, 164-171.

6. **Zhi Chang**, Yu Qiao, Jie Wang, Yibo He, Han Deng and Haoshen Zhou. Two-dimensional metal-organic framework with perpendicular one dimensional nano-channel as precise polysulfides sieves for high efficient lithium−sulfur batteries. **Submitted to Small**.

7. **Zhi Chang**, Yu Qiao, Huijun Yang, Han Deng, Ping He and Haoshen Zhou. Achieving ultrathin solid-electrolyte-interphase on dendrite-free lithium-metal anode

by a highly-aggregated electrolyte interlayer. **In preparation**.

8. Huijun Yang[+], **Zhi Chang[+]** (Co-first author), Yu Qiao, Han Deng, Xiaowei Mu, Ping He and Haoshen Zhou. Constructing a over-saturated electrolyte front surface for stable rechargeable aqueous zinc batteries. *Angew. Chem. Int. Ed.*, DOI: 10.1002/anie.202001844.

9. Jie Wang, **Zhi Chang[+]** (Co-first author), Bing Ding, Yusuke Ide, and Yusuke Yamauchid. A universal strategy to heterostructure of 2D materials with single-layer ordered mesoporous materials. *Angew. Chem. Int. Ed.* (Accepted).

10. Yibo He[+], **Zhi Chang[+]** (Co-first author), Shichao Wu, Haoshen Zhou. Effective strategies for long-cycle life lithium-sulfur batteries. *Journal of Materials Chemistry A*, 2018, 6, (15), 6155-6182.

Acknowledgements

Time fly so fast. I still remember the first day I come to Japan, the first day I join University of Tsukuba and AIST. During the past three-years study in Tsukuba, I have gained a lot in my life. Living and studying in Tsukuba is really an interesting and unforgettable memory for me. I love the peaceful atmosphere and slow pace of life here. Yet, happy life is always short, it's time to say goodbye to the past days. At the end of my three-year doctoral course, I am deeply grateful for those who have offered help, give guidance and support on my studying and living.

First of all, I would like to give my sincerely gratitude to my supervisor Professor Haoshen Zhou (from University of Tsukuba and AIST) for his patient guidance, instillation and continued support during the past three years. He is a really nice and wisdom man and always willing to share his ideas and opinions with me, which I think is absolutely help to me. He always encourages me to go step further in the field I major in. He is also a sharp-eyed researcher who is capable to focus on some seemed "minor issues" and encourage us to dig them further. He also patiently helps me a lot during the writing of my research papers to further polish my work. I will never forget his rigorous attitude towards science.

Then, I would like to give my gratitude to my two vice-supervisors at University of Tsukuba, Prof. Masayoshi Ishida and Associate Prof. Hirohisa Aki. Every time we visit them in their office, they always help us intimately and ask us how our lives are in Tsukuba. Really appreciate about it. Particularly, thanks to the suggestions of Prof. Masayoshi Ishida, Associate Prof. Takayasu Fujino, Associate Prof. Hirohisa Aki and Dr. Hirokazu Kitaura on my graduation presentation, it makes my presentation improved significantly.

Thirdly, I want to express my sincere gratitude to Dr. Yu Qiao. He helps me a lot

during the past three years. He is a high-level scientific research worker with solid theoretical foundation and is proficient in various characterization methods. He guided me in designing experiments, characterizing samples and analyzing results. He willing to share his opinions and suggestions with me which can further polish my work. His hardworking impressed me a lot. I have learned a lot from him.

Fourth, many thanks to all my group numbers in AIST. Dr. Hirofumi Matsuda, Dr. Eunjoo Yoo, Dr. Hirokazu Kitaura and Mr. Jun Okagaki gave lots of help when I work in AIST. I also would like to thank Ms Y. Okita-san, our secretary who helps us a lot in every daily thing. She is such a good and yasashi madam and always willing to give her hand to us at any time. I want to thank Dr. Yarong Wang, Dr. Shichao Wu, Dr. Xiang Li, Dr. Linlin Wang, Dr. Feilong Qiu, Mr. Xin Cao and Mr, Xingyu Zhu, Prof. Jianan Zhang and Prof. Anqiang Pan, they gave suggestions and assistance on my life and study. I also would like to thank my classmate and friend Mr. Han Deng and Ms. Min Jia. We come to Tsukuba from China together three years ago. We go to class and our lab in AIST together and mutual encourage each other. We also spend plentiful as well as wonderful memories when we travel to several beautiful places in Japan. It means a lot to me and I will treasure them forever in the rest of my life. I also want to thank Mr. Huijun Yang for accompanying me to ride around the villages, rivers and lakes in Tsukuba and Tsuchiura. I also would like to thank him for sharing scientific opinions and suggestions as well as interesting things in our lives. Really appreciate about it. I would also like to thank Dr. Bing Ding, Dr. Jie Wang and Mr. Gaoliang Yang in NIMS. We know each other since six years ago. Really appreciate their unselfish and valuable suggestions and help.

Furthermore, I would like to thank the financial support provided by the China Scholarship Council.

Lastly, I am deeply indebted to my family. My father Pingyu Chang, my mother

Jinrong Wang, my elder sister Hui Chang and my little brother Yong Chang support me for my entire doctoral program. Especially, I would like to thank my girlfriend Sijie Li. We fall in love at the end of my PhD period, thank you very much for your love and trust. Your love and encouragements make me a better man. I am looking forward to share the rest of my life with you.

References

1. Scharber, M. C.; Mühlbacher, D.; Koppe, M.; Denk, P.; Waldauf, C.; Heeger, A. J.; Brabec, C. J. *Advanced materials* **2006,** 18, (6), 789-794.

2. Koutroulis, E.; Kalaitzakis, K. *IEEE transactions on industrial electronics* **2006,** 53, (2), 486-494.

3. Aqeel, A.; Butt, M. S. *Asia-Pacific Development Journal* **2001,** 8, (2), 101-110.

4. Casals, L. C.; García, B. A. In *A review of the complexities of applying second life electric car batteries on energy businesses*, Energy Syst. Conf, 2014.

5. Tsujikawa, T.; Yabuta, K.; Arakawa, M.; Hayashi, K. *Journal of power sources* **2013,** 244, 11-16.

6. Armand, M.; Tarascon, J. M. *Nature* **2008,** 451, (7179), 652-657.

7. Xia, H.; Luo, Z.; Xie, J. *Progress in Natural Science: Materials International* **2012**, 22, (6), 572-584.

8. Goodenough, J. B.; Park, K. S. *Journal of the American Chemical Society* **2013,** 135, (4), 1167-1176.

9. Tarascon, J.; Armand, M. *Nature* **2001,** 414, (6861), 359-367.

10. Goodenough, J. B.; Kim, Y. *Chemistry of Materials* **2010,** 22, (3), 587-603.

11. Marom, R.; Amalraj, S.; Leifer, N.; Jacob, D.; Aurbach, D. *Journal of Materials Chemistry* **2011,** 21, (27), 9938-9954.

12. Scrosati, B.; Garche, J. *Journal of Power Sources* **2010,** 195, (9), 2419-2430.

13. Bachman, J. C.; Muy, S.; Grimaud, A.; Chang, H. H.; Pour, N.; Lux, S. F.; Paschos, O.; Maglia, F.; Lupart, S.; Lamp, P.; Giordano, L.; Shao-Horn, Y. *Chem Rev* **2016,** 116, (1), 140-62.

14. Cao, R.; Xu, W.; Lv, D.; Xiao, J.; Zhang, J.-G. *Advanced Energy Materials* **2015,** 5, (16).

15. Cheng, X. B.; Zhang, R.; Zhao, C. Z.; Zhang, Q. *Chem Rev* **2017,** 117, (15), 10403-10473.

16. http://www.pasticheenergysolutions.com/applications/.

17. Li, Z.; Huang, J.; Yann Liaw, B.; Metzler, V.; Zhang, J. *Journal of Power Sources* **2014,** 254, 168-182.

18. Etacheri, V.; Marom, R.; Elazari, R.; Salitra, G.; Aurbach, D. *Energy & Environmental Science* **2011,** 4, (9), 3243-3262.

19. Bonaccorso, F.; Colombo, L.; Yu, G.; Stoller, M.; Tozzini, V.; Ferrari, A. C.; Ruoff, R. S.; Pellegrini, V. *Science* **2015,** 347, (6217).

20. Xu, K. *Chemical reviews* **2004,** 104, (10), 4303-4418.

21. Xu, K. *Chem Rev* **2014,** 114, (23), 11503-618.

22. Suo, L.; Borodin, O.; Gao, T.; Olguin, M.; Ho, J.; Fan, X.; Luo, C.; Wang, C.; Xu, K. *Science* **2015,** 350, (6263), 938-43.

23. Yamada, Y.; Wang, J.; Ko, S.; Watanabe, E.; Yamada, A. *Nature Energy* **2019**.

24. Lin, D.; Liu, Y.; Cui, Y. *Nat Nanotechnol* **2017,** 12, (3), 194-206.

25. Tikekar, M. D.; Choudhury, S.; Tu, Z.; Archer, L. A. *Nature Energy* **2016,** 1, (9).

26. Tu, Z.; Nath, P.; Lu, Y.; Tikekar, M. D.; Archer, L. A. *Acc Chem Res* **2015,** 48, (11), 2947-56.

27. Wood, K. N.; Noked, M.; Dasgupta, N. P. *ACS Energy Letters* **2017,** 2, (3), 664-672.

28. Xu, W.; Wang, J.; Ding, F.; Chen, X.; Nasybulin, E.; Zhang, Y.; Zhang, J.-G. *Energy Environ. Sci.* **2014,** 7, (2), 513-537.

29. Younesi, R.; Veith, G. M.; Johansson, P.; Edström, K.; Vegge, T. *Energy & Environmental Science* **2015,** 8, (7), 1905-1922.

30. Qiao, Y.; Deng, H.; He, P.; Zhou, H. *Joule* **2020**.

31. Feng, S.; Lunger, J. R.; Johnson, J. A.; Shao-Horn, Y. *Science* **2018,** 361, (6404),

758.

32. Ding, F.; Xu, W.; Chen, X.; Zhang, J.; Engelhard, M. H.; Zhang, Y.; Johnson, B. R.; Crum, J. V.; Blake, T. A.; Liu, X.; Zhang, J.-G. *Journal of The Electrochemical Society* **2013,** 160, (10), A1894-A1901.

33. Fan, X.; Chen, L.; Borodin, O.; Ji, X.; Chen, J.; Hou, S.; Deng, T.; Zheng, J.; Yang, C.; Liou, S. C.; Amine, K.; Xu, K.; Wang, C. *Nat Nanotechnol* **2018,** 13, (8), 715-722.

34. Hood, Z. D.; Wang, H.; Samuthira Pandian, A.; Keum, J. K.; Liang, C. *J Am Chem Soc* **2016,** 138, (6), 1768-71.

35. Lithium Metal Anode. In *Encyclopedia of Inorganic and Bioinorganic Chemistry*, pp 1-21.

36. Gao, H.; Cai, J.; Xu, G.-L.; Li, L.; Ren, Y.; Meng, X.; Amine, K.; Chen, Z. *Chemistry of Materials* **2019,** 31, (8), 2723-2730.

37. Han, J. G.; Kim, K.; Lee, Y.; Choi, N. S. *Adv Mater* **2018**, e1804822.

38. Yu, Y.; Karayaylali, P.; Katayama, Y.; Giordano, L.; Gauthier, M.; Maglia, F.; Jung, R.; Lund, I.; Shao-Horn, Y. *The Journal of Physical Chemistry C* **2018,** 122, (48), 27368-27382.

39. Chang, Z.; Qiao, Y.; Deng, H.; Yang, H.; He, P.; Zhou, H. *Energy & Environmental Science* **2020,** 13, (4), 1197-1204.

40. Cao, X.; Ren, X.; Zou, L.; Engelhard, M. H.; Huang, W.; Wang, H.; Matthews, B. E.; Lee, H.; Niu, C.; Arey, B. W.; Cui, Y.; Wang, C.; Xiao, J.; Liu, J.; Xu, W.; Zhang, J.-G. *Nature Energy* **2019,** 4, (9), 796-805.

41. Chen, L.; Fan, X.; Hu, E.; Ji, X.; Chen, J.; Hou, S.; Deng, T.; Li, J.; Su, D.; Yang, X. *Chem* **2019,** 5, (4), 896-912.

42. Cheng, X.-B.; Yan, C.; Chen, X.; Guan, C.; Huang, J.-Q.; Peng, H.-J.; Zhang, R.; Yang, S.-T.; Zhang, Q. *Chem* **2017,** 2, (2), 258-270.

43. Jiao, S.; Ren, X.; Cao, R.; Engelhard, M. H.; Liu, Y.; Hu, D.; Mei, D.; Zheng, J.; Zhao, W.; Li, Q.; Liu, N.; Adams, B. D.; Ma, C.; Liu, J.; Zhang, J.-G.; Xu, W. *Nature Energy* **2018,** 3, (9), 739-746.

44. Wang, J.; Yamada, Y.; Sodeyama, K.; Chiang, C. H.; Tateyama, Y.; Yamada, A. *Nat Commun* **2016,** 7, 12032.

45. Zheng, J.; Engelhard, M. H.; Mei, D.; Jiao, S.; Polzin, B. J.; Zhang, J.-G.; Xu, W. *Nature Energy* **2017,** 2, (3).

46. Lee, Y.; Lee, T. K.; Kim, S.; Lee, J.; Ahn, Y.; Kim, K.; Ma, H.; Park, G.; Lee, S.-M.; Kwak, S. K. *Nano Energy* **2020,** 67, 104309.

47. Suo, L.; Borodin, O.; Wang, Y.; Rong, X.; Sun, W.; Fan, X.; Xu, S.; Schroeder, M. A.; Cresce, A. V.; Wang, F. *Advanced Energy Materials* **2017,** 7, (21), 1701189.

48. Wang, Z.; Tan, R.; Wang, H.; Yang, L.; Hu, J.; Chen, H.; Pan, F. *Advanced Materials* **2018,** 30, (2), 1704436.

49. Hu, Z.; Zhang, S.; Dong, S.; Li, Q.; Cui, G.; Chen, L. *Chemistry of Materials* **2018,** 30, (12), 4039-4047.

50. Lu, Y.; Tikekar, M.; Mohanty, R.; Hendrickson, K.; Ma, L.; Archer, L. A. *Advanced Energy Materials* **2015,** 5, (9).

51. Bedrov, D.; Borodin, O.; Smith, G. D. *The Journal of Physical Chemistry B* **1998,** 102, (29), 5683-5690.

52. Chen, S.; Zheng, J.; Yu, L.; Ren, X.; Engelhard, M. H.; Niu, C.; Lee, H.; Xu, W.; Xiao, J.; Liu, J. *Joule* **2018,** 2, (8), 1548-1558.

53. Gao, Y.; Guo, M.; Yuan, K.; Shen, C.; Ren, Z.; Zhang, K.; Zhao, H.; Qiao, F.; Gu, J.; Qi, Y.; Xie, K.; Wei, B. *Advanced Energy Materials* **2020,** 10, (4), 1903362.

54. Shen, Y.; Zhang, Y.; Han, S.; Wang, J.; Peng, Z.; Chen, L. *Joule* **2018,** 2, (9), 1674-1689.

55. Srivastava, S.; Schaefer, J. L.; Yang, Z.; Tu, Z.; Archer, L. A. *Adv Mater* **2014,** 26,

(2), 201-34.

56. Zhang, P.; Zhao, Y.; Zhang, X. *Chem Soc Rev* **2018,** 47, (8), 2921-3004.

57. Banerjee, R.; Phan, A.; Wang, B.; Knobler, C.; Furukawa, H.; O'Keeffe, M.; Yaghi, O. M. *Science* **2008,** 319, (5865), 939-943.

58. Hou, Q.; Wu, Y.; Zhou, S.; Wei, Y.; Caro, J.; Wang, H. *Angew Chem Int Ed Engl* **2019,** 58, (1), 327-331.

59. Peng, Y.; Li, Y.; Ban, Y.; Jin, H.; Jiao, W.; Liu, X.; Yang, W. *Science* **2014,** 346, (6215), 1356-9.

60. de Lima, G. F.; Mavrandonakis, A.; de Abreu, H. A.; Duarte, H. A.; Heine, T. *The Journal of Physical Chemistry C* **2013,** 117, (8), 4124-4130.

61. Wisser, D.; Wisser, F. M.; Raschke, S.; Klein, N.; Leistner, M.; Grothe, J.; Brunner, E.; Kaskel, S. *Angew Chem Int Ed Engl* **2015,** 54, (43), 12588-91.

62. Kalmutzki, M. J.; Diercks, C. S.; Yaghi, O. M. *Adv Mater* **2018,** 30, (37), e1704304.

63. Meunier, F. *Science* **2017,** 358, (6366).

64. Fathieh, F.; Kalmutzki, M. J.; Kapustin, E. A.; Waller, P. J.; Yang, J.; Yaghi, O. M. *Science advances* **2018,** 4, (6), eaat3198.

65. Miner, E. M.; Park, S. S.; Dinca, M. *J Am Chem Soc* **2019,** 141, (10), 4422-4427.

66. Shen, L.; Wu, H. B.; Liu, F.; Brosmer, J. L.; Shen, G.; Wang, X.; Zink, J. I.; Xiao, Q.; Cai, M.; Wang, G.; Lu, Y.; Dunn, B. *Adv Mater* **2018,** 30, (23), e1707476.

67. Chen, H.; Tu, H.; Hu, C.; Liu, Y.; Dong, D.; Sun, Y.; Dai, Y.; Wang, S.; Qian, H.; Lin, Z.; Chen, L. *J Am Chem Soc* **2018,** 140, (3), 896-899.

68. Xu, Q.; Tao, S.; Jiang, Q.; Jiang, D. *J Am Chem Soc* **2018,** 140, (24), 7429-7432.

69. Zhang, Y.; Duan, J.; Ma, D.; Li, P.; Li, S.; Li, H.; Zhou, J.; Ma, X.; Feng, X.; Wang, B. *Angew Chem Int Ed Engl* **2017,** 56, (51), 16313-16317.

70. Bai, S.; Sun, Y.; Yi, J.; He, Y.; Qiao, Y.; Zhou, H. *Joule* **2018,** 2, (10), 2117-2132.

71. Bai, S.; Liu, X.; Zhu, K.; Wu, S.; Zhou, H. *Nature Energy* **2016,** 1, (7), 16094.

72. Cui, S.; Qin, M.; Marandi, A.; Steggles, V.; Wang, S.; Feng, X.; Nouar, F.; Serre, C. *Sci Rep* **2018,** 8, (1), 15284.

73. Bennett, T. D.; Cheetham, A. K.; Fuchs, A. H.; Coudert, F. X. *Nat Chem* **2016,** 9, (1), 11-16.

74. Cheng, Y.; Ying, Y.; Japip, S.; Jiang, S. D.; Chung, T. S.; Zhang, S.; Zhao, D. *Adv Mater* **2018,** 30, (47), e1802401.

75. Furukawa, H.; Cordova, K. E.; O'Keeffe, M.; Yaghi, O. M. *Science* **2013,** 341, (6149), 1230444.

76. Wang, X.; Chen, L.; Chong, S. Y.; Little, M. A.; Wu, Y.; Zhu, W. H.; Clowes, R.; Yan, Y.; Zwijnenburg, M. A.; Sprick, R. S.; Cooper, A. I. *Nat Chem* **2018,** 10, (12), 1180-1189.

77. Yang, F.; Xu, G.; Dou, Y.; Wang, B.; Zhang, H.; Wu, H.; Zhou, W.; Li, J.-R.; Chen, B. *Nature Energy* **2017,** 2, (11), 877-883.

78. Gascon, J. *Science* **2017,** 358, (6361), 303.

79. Rodenas, T.; Luz, I.; Prieto, G.; Seoane, B.; Miro, H.; Corma, A.; Kapteijn, F.; Llabres, I. X. F. X.; Gascon, J. *Nat Mater* **2015,** 14, (1), 48-55.

80. Vallejos-Burgos, F.; Coudert, F. X.; Kaneko, K. *Nat Commun* **2018,** 9, (1), 1812.

81. Xie, K.; Fu, Q.; Xu, C.; Lu, H.; Zhao, Q.; Curtain, R.; Gu, D.; Webley, P. A.; Qiao, G. G. *Energy & Environmental Science* **2018,** 11, (3), 544-550.

82. Canivet, J.; Fateeva, A.; Guo, Y.; Coasne, B.; Farrusseng, D. *Chem Soc Rev* **2014,** 43, (16), 5594-617.

83. Kapustin, E. A. *Chem* **2018,** 4, (1), 16-17.

84. Fujie, K.; Ikeda, R.; Otsubo, K.; Yamada, T.; Kitagawa, H. *Chemistry of Materials* **2015,** 27, (21), 7355-7361.

85. Guo, Z.; Zhang, Y.; Dong, Y.; Li, J.; Li, S.; Shao, P.; Feng, X.; Wang, B. *J Am*

Chem Soc **2019,** 141, (5), 1923-1927.

86. Wang, Z.; Wang, Z.; Yang, L.; Wang, H.; Song, Y.; Han, L.; Yang, K.; Hu, J.; Chen, H.; Pan, F. *Nano Energy* **2018,** 49, 580-587.

87. Liu, X.; Li, X.; Li, H.; Wu, H. B. *Chemistry* **2018,** 24, (69), 18293-18306.

88. DeCoste, J. B.; Denny, M. S., Jr.; Peterson, G. W.; Mahle, J. J.; Cohen, S. M. *Chem Sci* **2016,** 7, (4), 2711-2716.

89. Gutiérrez-Sevillano, J. J.; Vicent-Luna, J. M.; Dubbeldam, D.; Calero, S. *The Journal of Physical Chemistry C* **2013,** 117, (21), 11357-11366.

90. Zhang, C.; Shen, L.; Shen, J.; Liu, F.; Chen, G.; Tao, R.; Ma, S.; Peng, Y.; Lu, Y. *Advanced Materials* **2019,** 31, (21), 1808338.

91. Denny, M. S., Jr.; Cohen, S. M. *Angew Chem Int Ed Engl* **2015,** 54, (31), 9029-32.

92. Fan, H.; Mundstock, A.; Feldhoff, A.; Knebel, A.; Gu, J.; Meng, H.; Caro, J. *J Am Chem Soc* **2018,** 140, (32), 10094-10098.

93. Moreton, J. C.; Denny, M. S.; Cohen, S. M. *Chem Commun (Camb)* **2016,** 52, (100), 14376-14379.

94. Qiao, Y.; Jiang, K.; Li, X.; Deng, H.; He, Y.; Chang, Z.; Wu, S.; Guo, S.; Zhou, H. *Advanced Energy Materials* **2018,** 8, (24), 1801120.

95. Xu, R.; Xiao, Y.; Zhang, R.; Cheng, X.-B.; Zhao, C.-Z.; Zhang, X.-Q.; Yan, C.; Zhang, Q.; Huang, J.-Q. *Advanced Materials* **2019,** 31, (19), 1808392.

96. Xue, W.; Shi, Z.; Huang, M.; Feng, S.; Wang, C.; Wang, F.; Lopez, J.; Qiao, B.; Xu, G.; Zhang, W. *Energy & Environmental Science* **2020**.

97. Shi, P.; Cheng, X.-B.; Li, T.; Zhang, R.; Liu, H.; Yan, C.; Zhang, X.-Q.; Huang, J.-Q.; Zhang, Q. *Advanced Materials* **2019,** 31, (37), 1902785.

98. Zeng, Z.; Murugesan, V.; Han, K. S.; Jiang, X.; Cao, Y.; Xiao, L.; Ai, X.; Yang, H.; Zhang, J.-G.; Sushko, M. L.; Liu, J. *Nature Energy* **2018,** 3, (8), 674-681.

99. Chen, S.; Zheng, J.; Mei, D.; Han, K. S.; Engelhard, M. H.; Zhao, W.; Xu, W.; Liu, J.; Zhang, J. G. *Advanced Materials* **2018,** 30, (21), 1706102.

100. Cho, S.-J.; Yu, D.-E.; Pollard, T. P.; Moon, H.; Jang, M.; Borodin, O.; Lee, S.-Y. *iScience* **2020,** 23, (2), 100844.

101. Fan, X.; Chen, L.; Ji, X.; Deng, T.; Hou, S.; Chen, J.; Zheng, J.; Wang, F.; Jiang, J.; Xu, K.; Wang, C. *Chem* **2018,** 4, (1), 174-185.

102. Qiu, F.; Li, X.; Deng, H.; Wang, D.; Mu, X.; He, P.; Zhou, H. *Advanced Energy Materials* **2019,** 9, (6), 1803372.

103. Suo, L.; Xue, W.; Gobet, M.; Greenbaum, S. G.; Wang, C.; Chen, Y.; Yang, W.; Li, Y.; Li, J. *Proc Natl Acad Sci U S A* **2018,** 115, (6), 1156-1161.

104. Yoshida, K.; Tsuchiya, M.; Tachikawa, N.; Dokko, K.; Watanabe, M. *The Journal of Physical Chemistry C* **2011,** 115, (37), 18384-18394.

105. Jeong, S.-K.; Seo, H.-Y.; Kim, D.-H.; Han, H.-K.; Kim, J.-G.; Lee, Y. B.; Iriyama, Y.; Abe, T.; Ogumi, Z. *Electrochemistry communications* **2008,** 10, (4), 635-638.

106. Battisti, D.; Nazri, G.; Klassen, B.; Aroca, R. *The Journal of Physical Chemistry* **1993,** 97, (22), 5826-5830.

107. Doi, T.; Shimizu, Y.; Hashinokuchi, M.; Inaba, M. *Journal of The Electrochemical Society* **2017,** 164, (1), A6412.

108. Qiao, Y.; Yi, J.; Guo, S.; Sun, Y.; Wu, S.; Liu, X.; Yang, S.; He, P.; Zhou, H. *Energy & Environmental Science* **2018,** 11, (5), 1211-1217.

109. Sonoki, H.; Matsui, M.; Imanishi, N. *Journal of The Electrochemical Society* **2019,** 166, (15), A3593.

110. Fan, X.; Chen, L.; Borodin, O.; Ji, X.; Chen, J.; Hou, S.; Deng, T.; Zheng, J.; Yang, C.; Liou, S.-C. *Nature nanotechnology* **2018,** 13, (8), 715-722.

111. Yang, H.; Chang, Z.; Qiao, Y.; Deng, H.; Mu, X.; He, P.; Zhou, H. *Angew. Chem. It. Ed.* **2020**, 59, (24), 9377-9381.